NASA TECHNICAL MEMORANDUM

NASA TM X-53557

1966

NASA TM X-53557

THERMOPHYSICS RESEARCH AT MSFC

RESEARCH ACHIEVEMENTS REVIEW

VOLUME II REPORT NO. 2

RESEARCH AND DEVELOPMENT OPERATIONS

GEORGE C. MARSHALL SPACE FLIGHT CENTER

HUNTSVILLE, ALABAMA

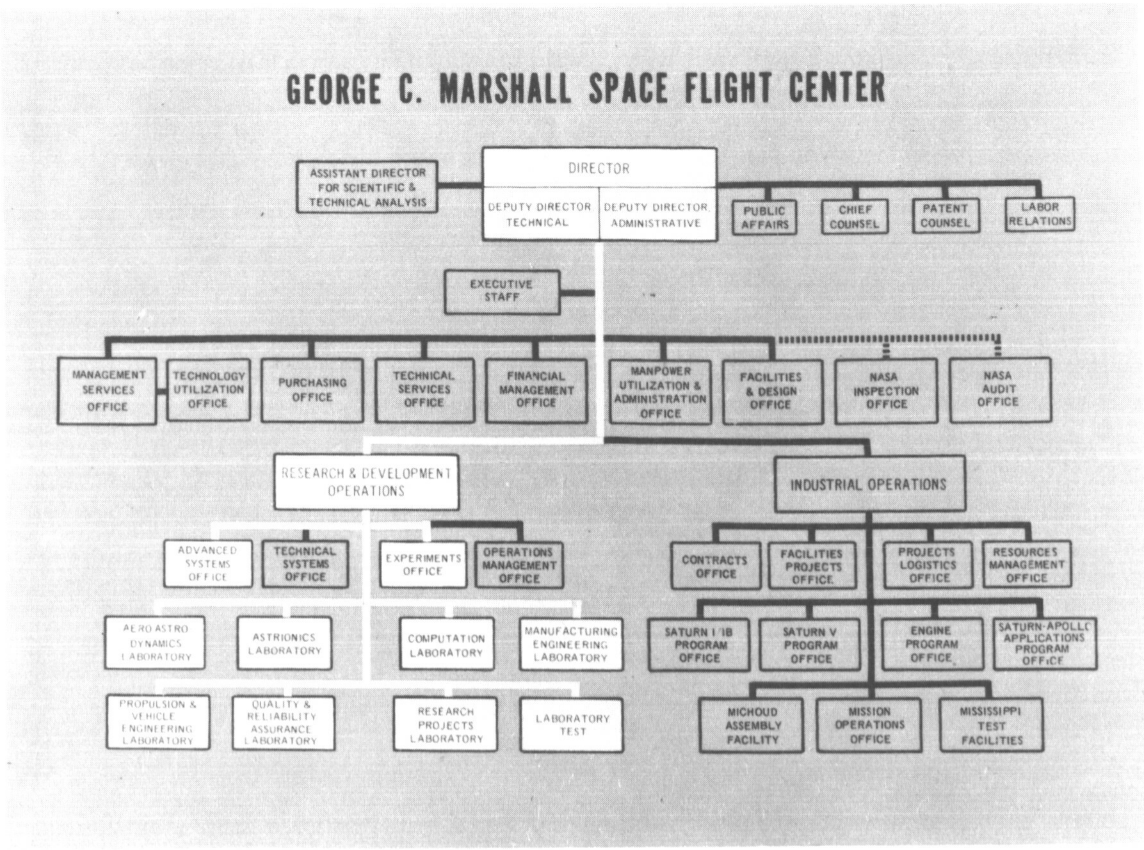

RESEARCH ACHIEVEMENTS REVIEWS COVER
THE FOLLOWING
FIELDS OF RESEARCH

- Radiation Physics
- Thermophysics
- Chemical Propulsion
- Cryogenic Technology
- Electronics
- Control Systems
- Materials
- Manufacturing
- Ground Testing
- Quality Assurance and Checkout
- Environmental and Aerodynamics
- Atmospheric Dynamics
- Instrumentation
- Power Systems
- Guidance Concepts
- Astrodynamics
- Advanced Tracking Systems
- Communication Systems
- Structures
- Mathematics and Computation
- Advanced Propulsion
- Lunar and Meteoroid Physics

1136

NASA TM X-53557

NATIONAL AERONAUTICS AND SPACE ADMINISTRATION
WASHINGTON, D. C.

RESEARCH ACHIEVEMENTS REVIEW

VOLUME II REPORT NO. 2

THERMOPHYSICS RESEARCH AT MSFC

RESEARCH AND DEVELOPMENT OPERATIONS
GEORGE C. MARSHALL SPACE FLIGHT CENTER
HUNTSVILLE, ALABAMA

1966

PRECEDING PAGE BLANK NOT FILMED.

PREFACE

In February 1965, Dr. Ernst Stuhlinger, Director, Research Projects Laboratory, initiated a series of Research Achievements Reviews which set forth those achievements accomplished by the laboratories of the Marshall Space Flight Center. Each review covered one or two fields of research in a form readily usable by specialists, systems engineers and program managers. The review of February 24, 1966, completed this series. Each review has been documented in the "Research Achievements Review Series."

In March 1966, a second series of Research Achievements Reviews was initiated. This second series has emphasized research areas of greatest concentration of effort, of most rapid progress, or of most pertinent interest to our research community. These reviews are being documented and published as "Research Achievements Review Reports, Volume II." Volume II will cover the reviews extending from March 1966 through February 1968.

The papers in this report were presented March 31, 1966

William G. Johnson
Director, Experiments Office

CONTENTS. . .

PRECEDING PAGE BLANK NOT FILMED.

LIST OF ILLUSTRATIONS

LIST OF ILLUSTRATIONS

EMISSIVITY PHYSICS

by Edgar R. Miller

LIST OF TABLES

LIST OF ILLUSTRATIONS

CONTENTS (Continued) . . .

LIST OF TABLES

LIST OF ILLUSTRATIONS

CONTENTS (Continued) . . .

PEGASUS THERMAL EXPERIMENTAL RESULTS

by William C. Snoddy

LIST OF ILLUSTRATIONS

CONTENTS (Continued). . .

LIST OF TABLES

LIST OF ILLUSTRATIONS

CONTENTS (Concluded) . . .

INTRODUCTION TO RESEARCH ACHIEVEMENTS REVIEW ON THERMOPHYSICS RESEARCH AT MSFC

By

Gerhard B. Heller

N67-24642

Research on thermal problems is conducted by various laboratories at MSFC. The Research Achievements Review given a year ago covered an over-all summary of thermophysics research and achievements in 1964 or before [1]. In this research review, several of these subjects are presented in more detail and include the achievements of the past year. Emphasis is placed on thermophysics as it pertains to space flight, especially with regard to radiation exchange with the environment. Research on thermal problems of launch vehicles is also mentioned. Aero-Astrodynamics Laboratory and Propulsion and Vehicle Engineering Laboratory are studying rocket base heating due to the effects of rocket engine jets and plumes. Aero-Astrodynamics Laboratory is studying the flow fields generated by interaction of multiple rocket jets and the interaction with the surrounding air flow. Theories are being developed for radiative transfer from the rocket exhaust gases and from carbon particles in the S-IB and S-IC rocket engine plumes. Thermal engineering problems are involved in cryogenic research in connection with liquid hydrogen. This includes studies of zero-gravity heat transfer of liquid hydrogen. Research in these two areas by Aero-Astrodynamics and Propulsion and Vehicle Engineering Laboratories was included in earlier research review reports by members of these laboratories [2, 3]. Materials research on thermal control coatings by P& VE Laboratory was covered in the Research Achievements Review Series No. 7 [4].

Astrionics Laboratory is concerned with temperature measuring devices for flight on Saturn vehicles. A thermal environmental effects sensor developed for Research Projects Laboratory (RPL) has been described in Research Achievements Review Series No. 5 [5]. Results of the sensor measurements are presented in this series.

Research Projects Laboratory is presently concerned with thermophysics research of the thermal space environment and thermal control of space vehicles.

This review consists of five papers on the following subjects: thermal similitude by B. P. Jones, emissivity physics research by E. Miller, ultraviolet radiation effects on thermal control coatings by G. Arnett, evaluation of Pegasus thermal experiments by W. C. Snoddy (all of Research Projects Laboratory), and thermophysical instruments by H. Burke (of Astrionics Laboratory). The achievements covered in these papers are indicative of thermophysics research at Marshall, but are not a complete representation. A few examples follow.

Klaus Schocken of RPL has conducted research on the modes of heat transfer of underdense dielectric materials. Figure 1 shows that heat transfer as a function of bulk density has a distinct minimum. This is because radiative transfer decreases with increasing density; however, the transfer by interface conductance between the powder particles increases. Research is conducted theoretically and experimentally to determine the modes of heat transfer. Results of this work are also applicable to the conductance of lunar surface materials.

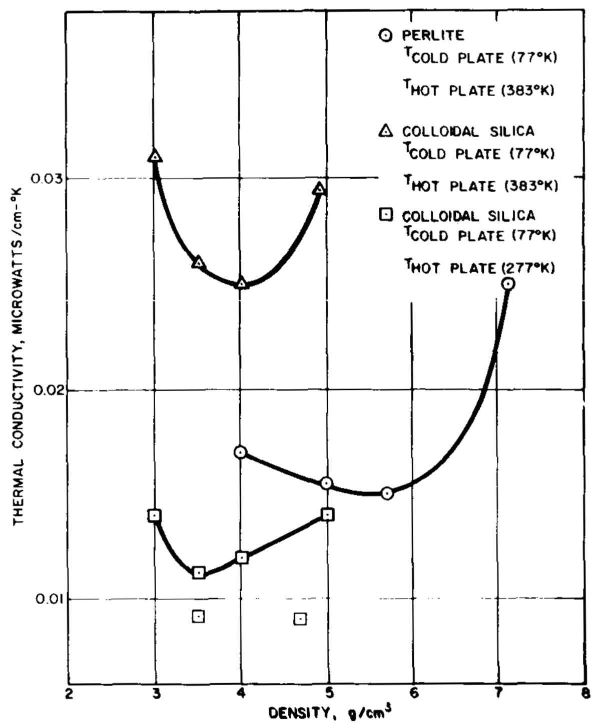

FIGURE 1. EFFECT OF CHANGE IN DENSITY ON THERMAL CONDUCTIVITY OF EVACUATED POWDERS

In the area of research on thermal control, Tommy Bannister of RPL has studied a space radiator using fusible materials. Figure 2 shows a laboratory model being studied by Northrop personnel under an MSFC contract. The fusible material is enclosed between two shells. Aluminum honeycomb is used to increase the heat conductivity between the upper and lower plate. In the experimental model a heater is mounted on the upper shell and the lower shell radiates to the liquid nitrogen-cooled walls of a vacuum chamber.

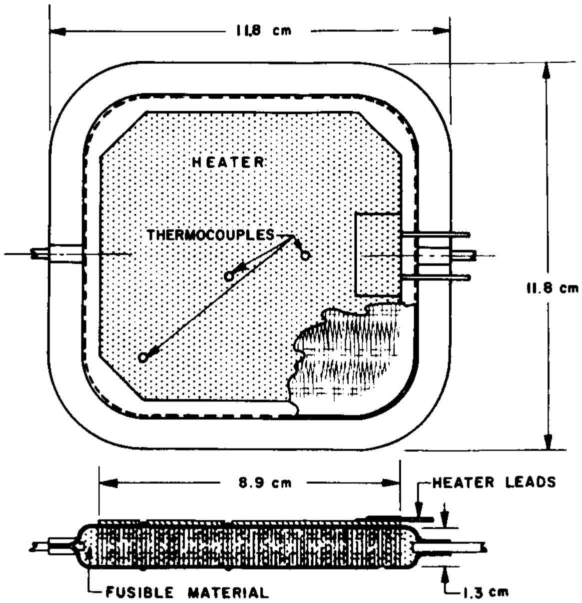

FIGURE 2. HEAT OF FUSION RADIATOR (ADIABATIC TEST MODEL)

A reversible heat storage device can be used to solve many problems resulting from the thermal environment of space. For example, a space thermal radiator, which would normally be sized for the extreme temperatures caused by the cyclic solar heating and cooling of a satellite eclipsed by the earth, could be designed for an average temperature by using a fusible material radiator. On Mars, where diurnal thermal variations are very severe, solar energy can be stored during the day to maintain moderate temperatures during the Martian night.

Laboratory studies are presently concentrated on improving the low thermal diffusivity of the liquid layer and reducing the expansion and contraction of fusible material between the liquid and solid state. A packaging technique has been developed that increases the thermal diffusivity while maintaining the fusible material in thermal contact with the heat source during all phases of operation.

REFERENCES

1. Thermophysics Research at MSFC. Research Achievements Review Series No. 2, NASA TM X-53490, 1965.

2. Cryogenics Research at MSFC. Research Achievements Review Series No. 3, NASA TM X-53515, 1965.

3. Terrestrial and Space Environment Research at MSFC. Research Achievements Review Series No. 11, NASA TM X-53507, 1965.

4. Materials Research at MSFC. Research Achievements Review Series No. 7, NASA TM X-53383, 1965.

5. Electronics Research at MSFC. Research Achievements Review Series No. 5, NASA TM X-53364, 1965.

EXPERIMENTAL RESULTS IN THERMAL SIMILITUDE

By

Billy P. Jones

SUMMARY

Earlier analytical work in thermal similitude is reviewed briefly to indicate the background and preparation for scale model experiments. Recent experimental results in thermal similarity are then presented. Results are included from experiments done by research contract with the Lockheed Missiles and Space Company and the ARO, Inc. Model design for the ARO, Inc., experiments was done inhouse.

Experimental confirmation was obtained for the derived modeling criteria for the transient mode. Geometric distortion in minor dimensions was found to be a useful technique, as predicted by the analysis.

The direction that future experimental and theoretical work should take is indicated.

INTRODUCTION

This presentation is primarily a summary of recent experimental results in thermal similitude. It is appropriate to briefly review the analytical work that preceded these experiments [1-5]. A large part of this analysis was done inhouse.

Earlier analytical work was concerned with the derivation of criteria for obtaining thermal similarity (the basis for thermal modeling). The considerations involved have well established analogies in wind tunnel testing to obtain information for aircraft design, model experiments to obtain data on the design of marine harbor and port facilities, and scale modeling of ships to obtain design information or to study their behavior under various conditions. Thermal modeling in space-related problems is a fairly recent activity.

SIMILITUDE RESULTS

DERIVATION OF CRITERIA

There are two established approaches to deriving the criteria for physical similarity. If descriptive differential equations can be written for the problem, the criteria can be derived from them. This approach has been used, and some of the experimental results discussed are for the purpose of verifying the derived modeling laws [2, 3, 5].

The other approach may be used when adequate descriptive equations are not available or when the equations are so complicated as to be difficult to treat. The method is based essentially on the so-called "π-Theorem." A recent reformulation of this principle was cast in the form of matrix algebra that can be programmed on a digital computer so that all possible sets of modeling criteria will be derived [1, 4]. In a relatively simple example for the temperature distribution with time in two opposed parallel disks connected by a rod, there resulted 57 sets of independent ratios, each set containing 5 ratios. Only one set is chosen for model design, but having all ratios exhibited allows the proper choice to be made. These two seemingly different approaches have connection through the group theory of abstract algebra that will be mentioned later.

EXPERIMENTAL VERIFICATION

The experimental results presented were obtained by research contract with the Lockheed Missiles and Space Company at Palo Alto, California, and the ARO, Inc., at Tullahoma under a Project SUPER arrangement with Arnold Engineering Development Center. Model design for the Tullahoma experiments was done inhouse. It was desirable to test our analysis by experiments to verify the derived thermal modeling laws. It was also necessary to learn some of the practical difficulties and techniques for designing, building, and testing models. All experiments used both a full-scale prototype and one or more scaled-down models, each tested under thermally similar conditions so that data could be compared for direct verification of the modeling. In addition, the analysis indicated that geometric distortion in the minor dimensions would be a useful technique in satisfying the modeling rules. This technique was used in the design of models when appropriate.

None of the experiments used actual flight hardware. However, the geometries, construction, materials, and thermal properties of the objects modeled did resemble simplified versions of situations that would be expected in actual hardware. The experiments proceeded from the simpler to the more complicated cases. All results presented are for transient conditions. Work at Marshall has concentrated on thermal problems that have time as a variable, thus time enters into the modeling criteria that must be satisfied. For this reason, the transient criteria are more difficult to satisfy than the corresponding criteria for the steady state.

EXPERIMENTAL APPARATUS AND DATA

Figure 1 shows the test installation for a cylinder, sphere and inclined plane exchanging energy by radiation only. The objects are asymmetrically located with respect to one another and there is mutual infrared shadowing. Solar insolation was simulated by resistance heaters in the plates, and internal generation was simulated by heaters in the cylinders. Tests on both a full-scale prototype and a one-half-scale model were run so that measurements could be compared [6].

Temperature-time curves are shown in Figure 2 for both model and prototype for each of the three objects. The heater in the plate was cycled with a period of about 4 hours, and the heater in the cylinder remained energized throughout the experiment. These figures show only one thermocouple location on each object, but they are fairly representative for the plate and cylinder. The curve shown for the sphere is representative of about one-half of all the measurements made on it.

The remainder of the experimental work discussed was done under a research contract by Robert E. Rolling at the Lockheed Missiles and Space Company, Palo Alto, California.

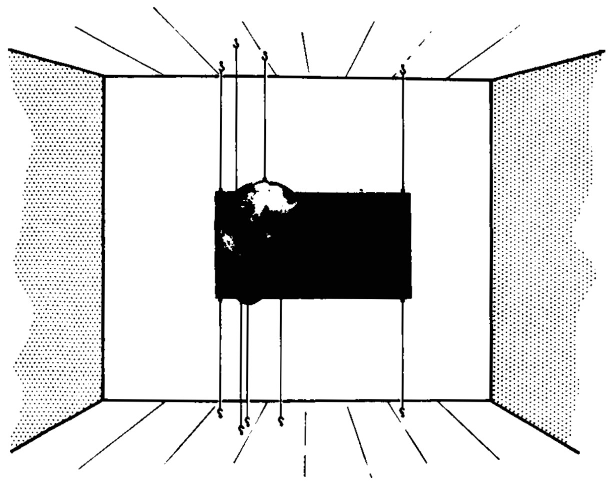

FIGURE 1. MODELS INSTALLED IN VACUUM CHAMBER

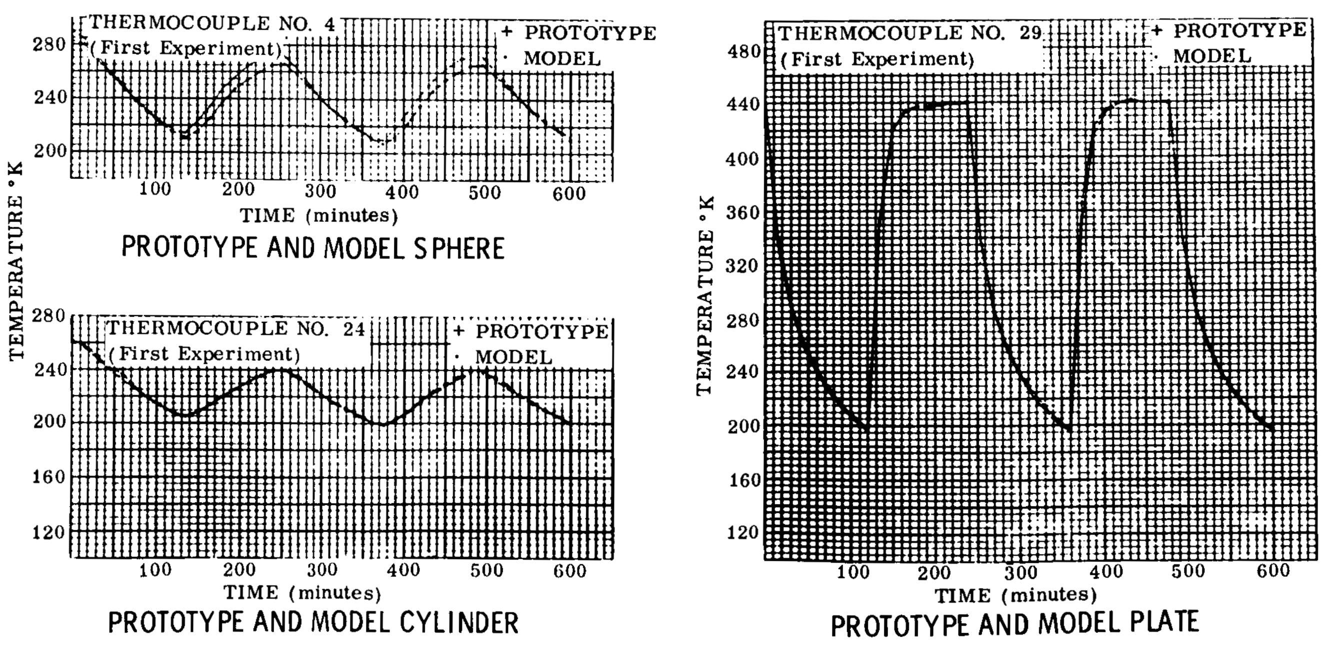

FIGURE 2. THERMAL SIMILITUDE - TULLAHOMA EXPERIMENTS

Figure 3 shows a prototype and two models, one model is $\frac{1}{2}$ scale, the other $\frac{1}{4}$ scale. They each consisted of two opposed disks with four connecting

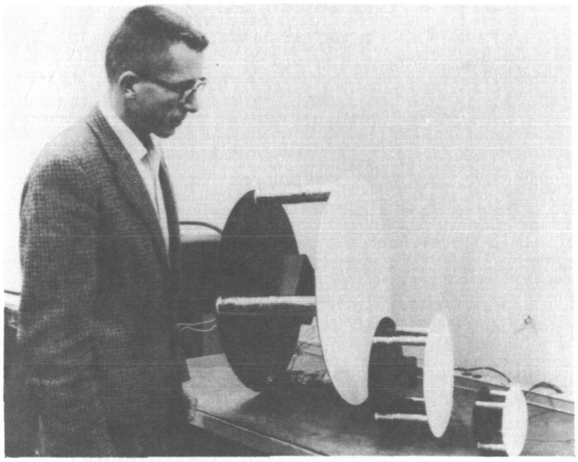

FIGURE 3. PROTOTYPE, $\frac{1}{2}$-SCALE AND $\frac{1}{4}$-SCALE MODELS

tubular members. An electric resistance heater was installed in the box attached to one of the disks. This was intended to simulate internal dissipation of equipment. The white surfaces were illuminated by an array of tungsten filament lamps with reflectors to simulate solar insolation. The internal heater was cycled with a period of 20 minutes. The external lamps were cycled with a period of 87 minutes.

Figures 4 and 5 are examples of the results which showed differences at the maximum, minimum, and average temperatures up to 9°K.

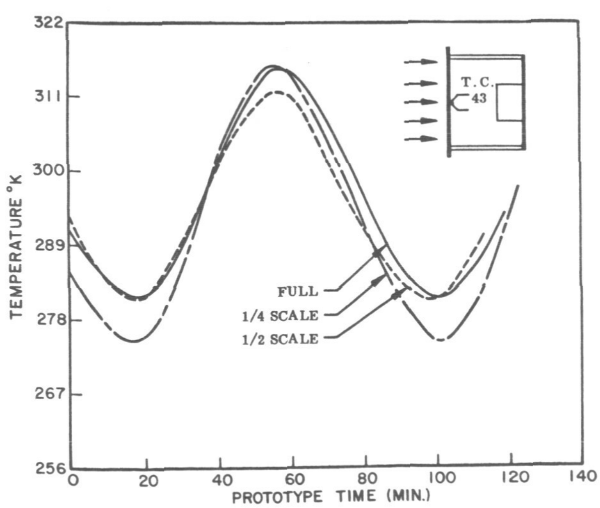

FIGURE 4. FRONT PLATE TEMPERATURE

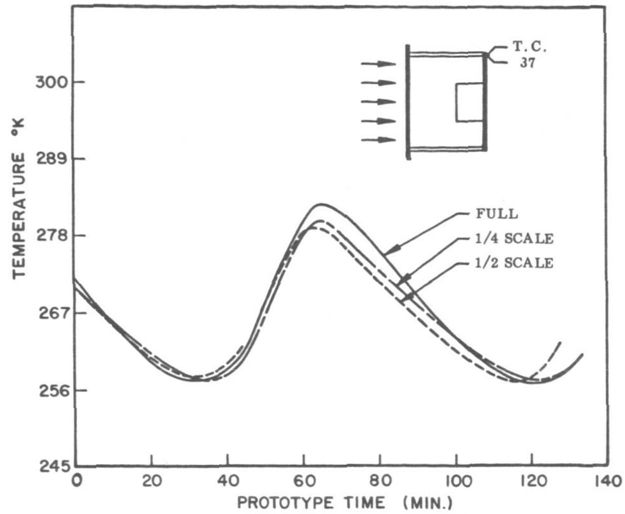

FIGURE 5. BACK PLATE EDGE TEMPERATURE

In the next series of experiments, a truncated cone-shaped object was used (Fig. 6). The full-scale cone height was 0.9144 meters (36 inches) and the base was 0.9144 meters (36 inches).

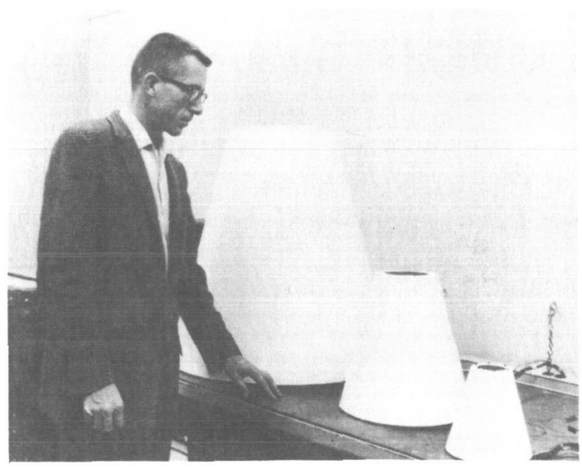

FIGURE 6. $\frac{1}{1}$-, $\frac{1}{2}$-, $\frac{1}{4}$-SCALE CONE MODELS

Four rods were mounted internally and ran the length of the cone (Fig. 7). Between two of the rods is a bare tungsten filament, and between the other two is a box with a heater inside. Again, $\frac{1}{2}$- and $\frac{1}{4}$-scale models were used.

An array of tungsten filament lamps with reflectors was again used to simulate solar insolation. In one set of experiments the base ends of the cones were

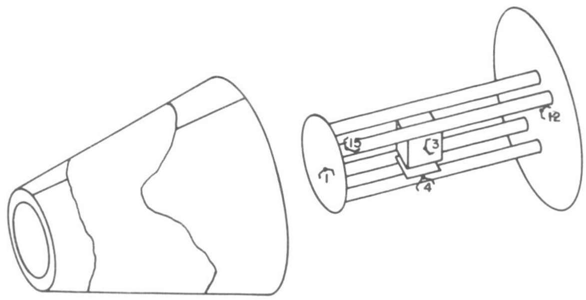

FIGURE 7. INTERNAL ARRANGEMENT

irradiated; in another set, the truncated ends were irradiated. Figure 8 shows the device used to rotate the cones for the two different sets of tests. They were rotated without disturbing the vacuum and low-temperature chamber wall conditions. Only some results of the set of tests where the bases were irradiated are given because the other results are of the same modeling quality.

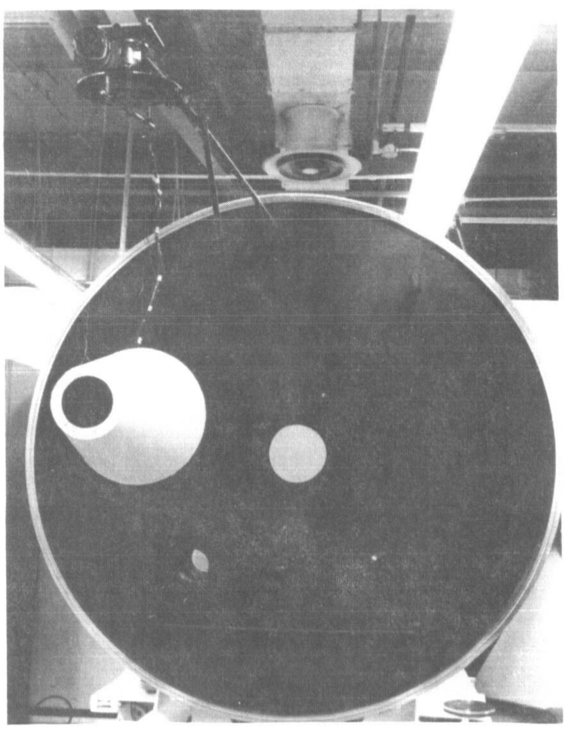

FIGURE 8. CONE INSTALLATION

Figure 9 shows the temperature-time curves for the prototype and both models for a measurement on the skin of the internal heater box enclosure. Figure 10 shows the results for a measurement which was

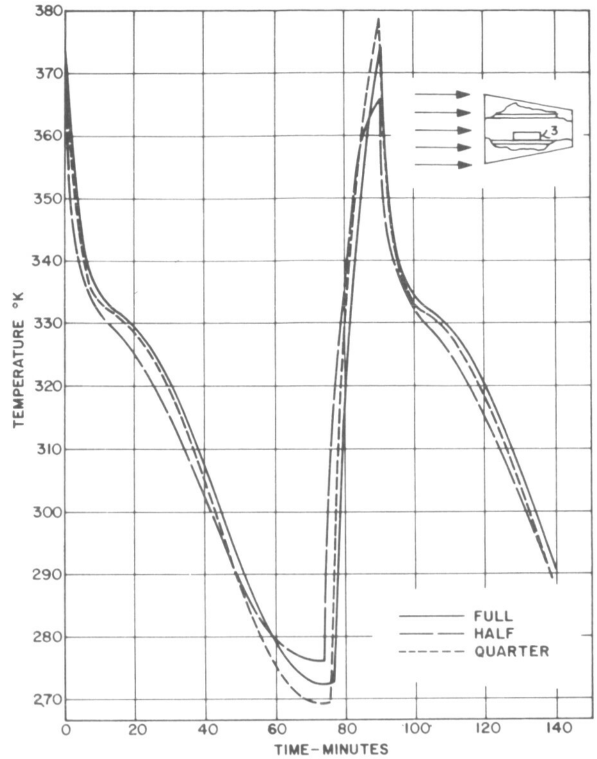

FIGURE 9. CONFIGURATION C - TRANSIENT THERMAL RESPONSE (T. C. No 3)

on the inside of the base at its geometric center. All results were within 8°K for both sets of tests between model and prototype.

CONCLUSION

Experimental confirmation was obtained for the derived thermal modeling criteria for the transient case for several situations that represent simplified versions in the thermal aspects of flight hardware. Geometric distortion in minor dimensions was found to be a useful technique in satisfying the criteria, and the work has identified some useful techniques for model design. Progress made in these experiments indicates that thermal similitude can be a useful addition to our methods of solving thermal problems during the design phase.

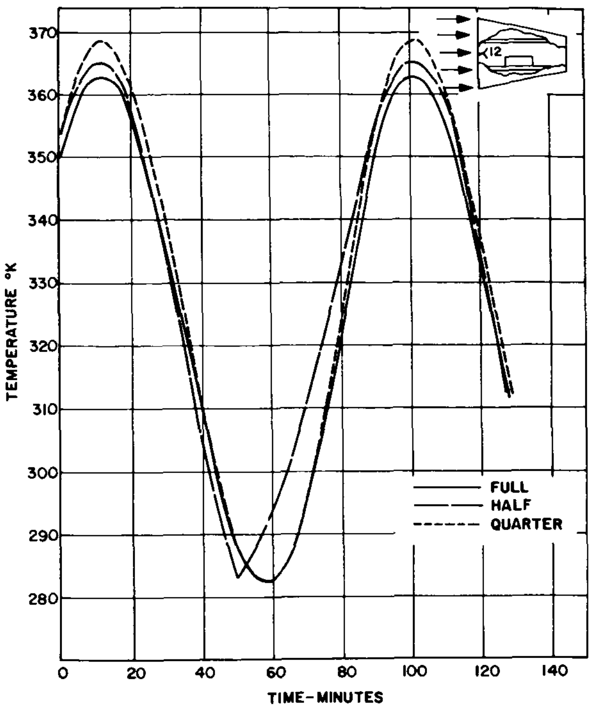

FIGURE 10. CONFIGURATION C - TRANSIENT THERMAL RESPONSE (T. C. No 12)

FUTURE RESEARCH

Future work should take two directions. First, more complicated configurations should be used in the scale modeling experiments. Second, further study should be made of the theoretical aspects. A skeleton for a unifying theory seems to exist through the concept of abstract groups. For example, Laszlo [8] has recently shown that a set of independent "π"-ratios for any particular physical problem forms the basis for a finite abelian group. Birkhoff [9] has already pointed out that the group theoretical concept underlies both the purely algebraic approach (e.g., the computer program discussed earlier) and the differential equations approach to the derivation of modeling criteria. In fact, such considerations have far-reaching implications in that they sometimes lead to a means for solving boundary value problems [10]. This can be important because many of the engineering and physics problems are stated in the form of partial differential equations together with certain boundary value conditions. There seems to be a fairly wide gap between the more abstract theory and everyday practices of modeling. It would be appropriate to do more research in this direction with the hope that results may be used to strengthen the applications side. Two research contracts that are slanted toward further research into the theory were recently initiated. One of them is with the University of Michigan, the other with Georgia Institute of Technology. Thus, future research in thermal similitude at Marshall takes both a theoretical and experimental direction.

REFERENCES

1. Watkins, J. R.: Thermal Similitude Using Brand's Theorem. Proceedings of Conference on Thermal Scale Modeling, NASA/OART, February 1964.

2. Jones, B. P.: Similitude Research in Space Vehicle Thermal Problems. Proceedings of Conference on Thermal Scale Modeling, NASA/OART, February 1964.

3. Jones, B. P.: Thermal Similitude Studies. Journal of Spacecraft and Rockets, Vol. 1, No. 4, July-August 1964.

4. Watkins, J. R.: Sets of Similarity Ratios for Thermal Modeling. NASA TND-3452, May 1966.

5. Rolling, R. E.: Results of Transient Thermal Modeling in a Simulated Space Environment. AIAA Thermophysics Specialist Conference, Paper No. 65-659, September 1965.

6. Jones, B. P.; and Harrison, J. K.: A Set of Experiments in Thermal Similitude. NASA TMX-53346, October 1965.

7. Rolling, R. E.: Thermal Modeling of a Truncated Cone in a Simulated Space Environment. AIAA Space Simulation Conference, September 1966.

8. Laszlo, A.: Systematization of Dimensionless Quantities by Group Theory. Int. J. Heat Mass Transfer, Vol. 7, 1964.

9. Birkhoff, G.: Hydrodynamics (A Study in Logic, Fact, and Similitude). Princeton University Press, 2nd ed., 1960.

10. Hansen, A.: Similarity Analysis of Boundary Value Problems in Engineering. Prentice Hall, Inc., 1964.

EMISSIVITY PHYSICS

By

Edgar R. Miller

N67-24644

SUMMARY

The activities of Research Projects Laboratory in emissivity physics have been primarily concerned with theoretical and experimental studies of optical and thermal control surface properties in the space environments. Various studies are presented to show some of the important problems in the area of thermal control coatings. The results of Research Projects Laboratory's theoretical and experimental work in many facets of emissivity physics are briefly discussed and appropriate references included.

INTRODUCTION

All space vehicle heat exchanges with its environment are radiative. The final average temperature of the space vehicle is a function of its absorption of these electromagnetic radiations and its ability to emit energy at these temperatures.

The sources of electromagnetic radiation are: 1) direct solar, 2) planetary reflection of solar energy, and 3) infrared radiations from planetary bodies and atmospheres.

Nearly all the thermal energy of solar radiation, either direct or indirect, is within the wavelengths of 0.2 to 3.0 micrometers, whereas the energy from planetary bodies and atmospheres is mainly contained in the 3.0- to about 50-micrometer region of the electromagnetic spectrum. This 3.0- to 50-micrometer region is also where most space vehicles must emit thermal energy.

The passive control of a space vehicle's temperature within desired limits depends on (1) how well the optical properties of the vehicle's thermal control surfaces are known and (2) the ability to understand and predict the effects of the space environments on the optical properties of these surfaces.

Much of our work in the area of emissivity physics has been centered upon the space environmental effects on the emissivity and optical absorption of thermal control surfaces and the associated problems of laboratory simulation and measurements.

These environments include: (1) low-energy charged particles of the solar wind, (2) solar electromagnetic radiation, and (3) micrometeoroids.

EFFECTS OF SOLAR WIND

The solar wind consists primarily of low-energy charged particles summarized in the following table.

TABLE I

FLUX, VELOCITY, AND ENERGY OF PRINCIPAL SOLAR WIND CONSTITUENTS

Particle	Constituents at One Astronomical Unit		
	Flux ($cm^{-2}sec^{-1}$)	Velocity (km/sec)	Energy (keV)
Proton (solar wind)	2×10^8	600	1.85
Proton (solar wind)	2×10^9	1000	5.0
α particle (solar wind)	3×10^7	600	7.4
α particle (solar wind)	3×10^8	1000	20

Figure 1 shows the optical degrading effects (in terms of change in solar absorptance) on the IIT Research Institute S-13 coating that consists of ZnO pigmented methyl silicone; this coating was used on the Pegasus satellites. The samples were bombarded

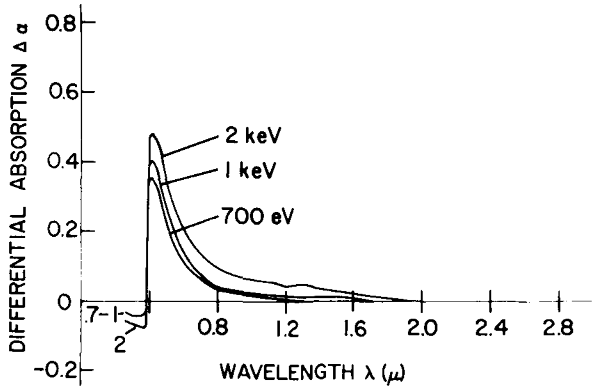

FIGURE 1. OPTICAL DEGRADING EFFECTS OF HYDROGEN ION BOMBARDMENT ON S-13

with ionic hydrogen gas (primarily H_2^+) in a duoplasmatron system. The hemispheric reflectance was measured in air before and after bombardment. Differential spectral absorptance was calculated from the reflectance data.

Figure 1 also shows the effect is increased with higher particle energy for the same integrated flux; this relation may not be true for higher energy regions where the penetration power is so great that the bulk rather than the optical surface is damaged.

Figure 2 shows the effect of helium (primarily He^+) bombardment on S-13 and Z-93 (ZnO pigmented K_2SiO_3) coatings. The Z-93 coating is to be used on the Apollo radiator. This figure points out two interesting phenomena. First, it is apparent that considerable damage is caused by the physical rather than chemical interaction of the particle, and physical rather than chemical interaction of the particle and the material. Second, the Z-93 is seen to be damaged considerably in the infrared region while the short wavelength absorption band is much narrower. This infrared damage is seen in ZnO powders and S-13 from in situ measurements after ultraviolet irradiation, while almost no effect is seen in Z-93 in this spectral region after ultraviolet irradiation and with in situ measurements. This will be discussed more fully under electromagnetic effects.

Finally, in Figure 3, the effects of particle mass are shown (velocity is kept constant). Because of less surface penetration power the heavier particle, with the exception of helium and hydrogen, is less effective in producing the degradation. This was also indicated by the data showing the effects of energy, the more energetic particles having a greater penetration depth and producing more damage. The samples shown in Figures 2 and 3 were bombarded in an r-f plasma chamber. The bombarding system and the work are fully described in [1, 2].

This work was done in conjunction with Dr. Wehner and Gordon Jorgenson at Litton Systems, Incorporated. Work was also performed on the theoretical aspects of optical absorption [3].

EFFECTS OF ELECTROMAGNETIC IRRADIATION

In situ measurements have only recently been performed on thermal control surfaces in connection with simulated space environments. It was discovered that severe degradation of solar reflectance is present on the S-13 coating system.

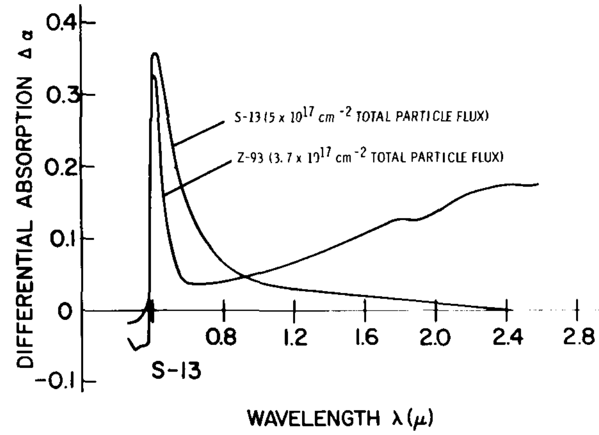

FIGURE 2. OPTICAL DEGRADING EFFECTS OF HELIUM ION BOMBARDMENT ON S-13 AND Z-93

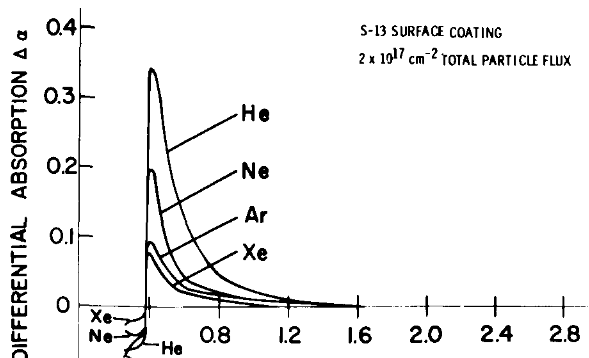

FIGURE 3. EFFECTS OF BOMBARDING PARTICLE MASS ON SURFACE CONTROL COATINGS

Figure 4 shows in situ bidirectional reflectance of S-13 before, during and after exposure to ultraviolet irradiation. It is seen that damage occurs very quickly in the infrared region and subsequent irradiation produces very little further damage. When air is readmitted to the chamber, full recovery is seen to occur and the sample regains its original reflective properties. The total integrated solar absorptance is calculated to change by about 40 percent,

Figure 5 shows the results of work performed inhouse in which the speed of the bleaching effect can be seen. The relative reflectance is monitored with a radiometer with a peak sensitivity at about 0.5 to 2.0 microns and air is admitted to the chamber to a pressure level of 130 newtons per square meter. In less than two minutes the samples have bleached more than 20 percent. Subsequent bleaching occurs when ambient pressure is admitted to the chamber.

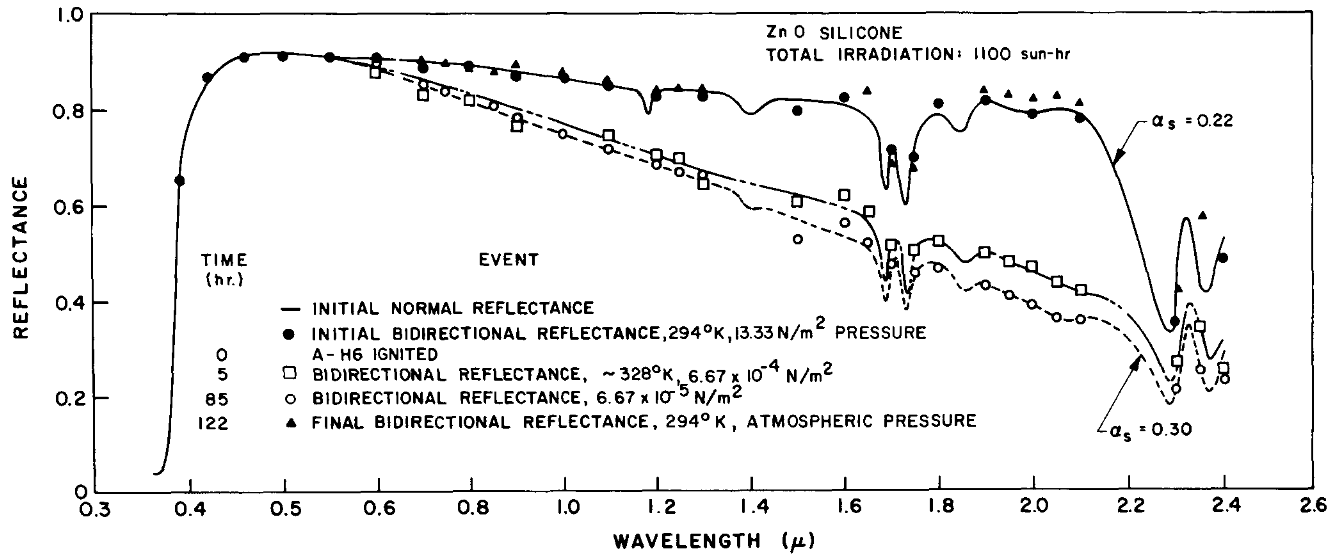

FIGURE 4. IN SITU SPECTRAL REFLECTANCE MEASUREMENTS ON ULTRAVIOLET IRRADIATED S-13

while if measured in the normal manner, i.e., taken out of the chamber and measured in air, almost no change would have been seen.

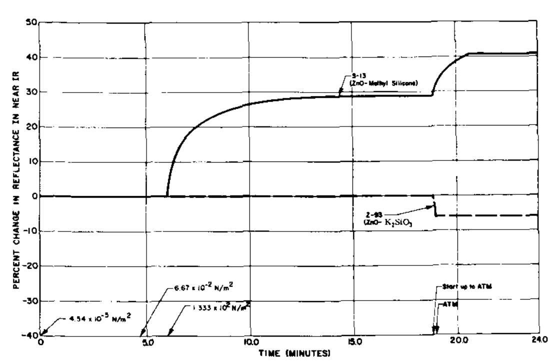

FIGURE 5. EFFECT OF ATMOSPHERIC EXPOSURE ON UV DEGRADED S-13 AND Z-93 COATINGS

The effect is not seen in the Z-93 coating system. In fact, there is a very slight increase in the in situ reflectance due to loss of water of hydration and consequent decreased water band absorption in this wavelength region. However, the damage to Z-93 by α particle simulation appears very similar to the damage seen in S-13 from in situ measurements, indicating that possibly some of the damage to Z-93 may have been masked since the measurements were taken in air before and after bombardment. Also indicated is the possible severe degradation by the combined environments of electromagnetic and solar wind irradiations.

The effect in ZnO and S-13 is thought to be photodesorption and adsorption of oxygen from the ZnO.

Additional work will be required in determining the effects of combined particulate and electromagnetic irradiations and performing in situ measurements of optical properties [2].

Much of this work was done under contract to Lockheed Missiles and Space Company [4] and is also being studied at IITRI [5].

MICROMETEOROID EFFECTS

Micrometeoroid erosion has demonstrated a significant effect on the optical properties of certain thermal control surfaces such as metallic coatings. Figure 6 shows increases in emittance from almost 0 to 100 percent, and solar absorptance increase up to 30 percent. These data are representative of the damage that might occur in a year at one astronomical unit.

THERMAL CONTROL SURFACES FLIGHT EXPERIMENT ON PEGASUS III

Figure 8 shows the mounting location of two of the eight coupons containing a total of 352 individual thermal control surface samples which were attached to the wing surfaces of Pegasus III in the hope that one day an astronaut could make in situ measurements and return the samples to earth for further laboratory studies. In situ measurements are

TOTAL DIRECTIONAL EMITTANCE (θ - 15^o) OF THE TEST SAMPLES

DESCRIPTION				EMITTANCE			SOLAR ABSORPTANCE		
	Materials	Impacts	% Coverage	Initial ϵ	After ϵ	Increase Δ^{ϵ}	Initial α	After α	Increase Δ^{α}
38-64	Gold	100,000	9.1	$.02_0$	$.02_1$	$.00_1$	$.23_7$	$.27_3$	$.03_6$
47-64	Gold	200,000	15.1	$.02_2$	$.02_8$	$.00_6$	$.23_2$	$.27_1$	$.03_9$
47-64	Gold	400,000	~30	$.02_0$	$.04_4$	$.02_4$	$.24_0$	$.29_3$	$.05_3$
51-64	304 Stainless Steel	300,000	~8	$.09_6$	$.11_4$	$.01_8$	$.45_4$	$.46_3$	$.00_9$
97-64	304 Stainless Steel	600,000	~16	$.10_3$	$.12_8$	$.02_5$	$.45_4$	$.48_3$	$.02_9$
40-64	Vacuum Deposited Aluminum	300,000	-	$.02_3$	$.04_0$	$.01_7$	$.11_0$	$.13_0$	$.02_0$
105-64	Vacuum Deposited Aluminum	600,000	-	$.03_0$	$.06_0$	$.03_0$	$.12_0$	$.15_8$	$.03_8$

FIGURE 6. EFFECT OF SIMULATED MICROMETEORITE BOMBARDMENT UPON INTEGRATED DIRECTIONAL REFLECTANCE

Perhaps an even more significant effect of meteoroid bombardment on optical properties is the introduction of a diffuse component on reflected radiation. Figure 7 gives the ratio of specular reflectance before and after bombardment. The performance of remote sensing and other optical components such as mirrors, lenses and windows will be significantly affected by such degradation.

Analytical models of the scattered light from meteoroid degraded surfaces are needed to more fully understand and predict the effects on systems performance. Thompson Ramo-Woolridge performed this work under contract from MSFC [6].

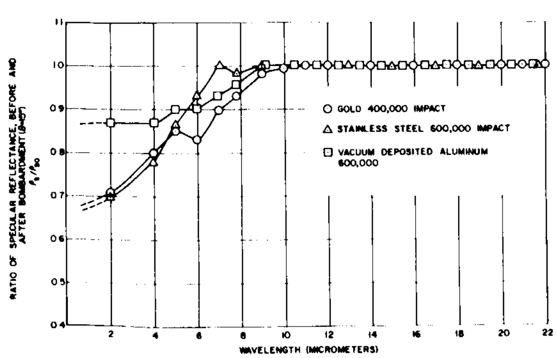

FIGURE 7. EFFECT OF MICROMETEOROID BOMBARDMENT UPON THE SPECULAR REFLECTANCE

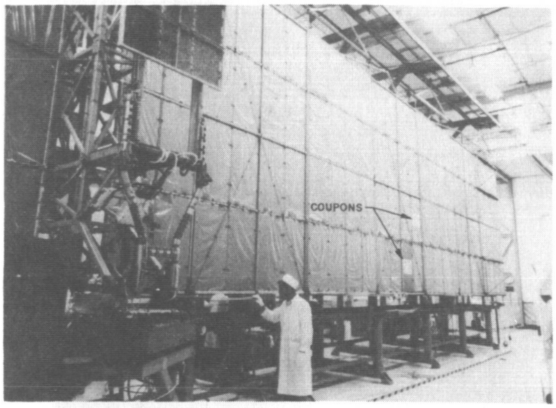

FIGURE 8. LOCATION OF THERMAL CONTROL SURFACE COUPONS ON PEGASUS III

necessary due to the anomalous infrared degradation exhibited by some thermal control surfaces upon ultraviolet irradiation which has been discussed previously. These samples represent the work of four NASA Centers, six private industries and industrial firms, one Army Ordnance Missile Laboratory and one foreign country.

The coatings on board have been flown or will be flown on Pegasus, Saturn, Apollo, Mariner, Lunar Orbiter and many others. Figure 9 shows a close-up of one of the coupons and the attached thermal control coating samples. Research Projects Laboratory collected the samples from the various contributors, catalogued, performed measurements, and mounted the samples to the coupons on very short notice.

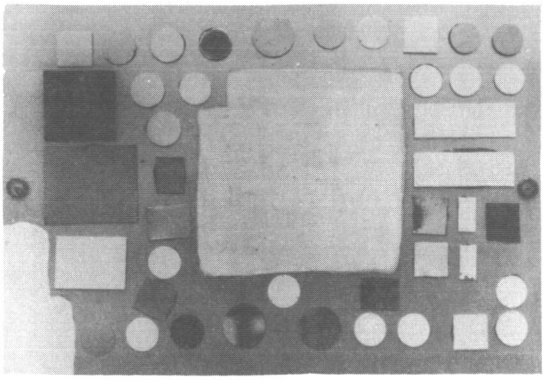

FIGURE 9. CLOSE-UP OF THERMAL CONTROL SURFACE COUPONS ON PEGASUS III

Although no definite plans have been made to recover these coupons, much valuable data will be obtained when such recovery is made.

Research Projects Laboratory is working on space-stable coatings of various types in conjunction with the Air Force (WADC) under Project SUPER [7]. Also, RPL is studying the theoretical directional back-scattering of oriented dielectric cylinders for possible use in thermal control [8].

Dr. Schocken of Research Projects Laboratory has studied the basic theory of emissivity and has found that the value of emissivity of metals under equilibrium conditions differs in the presence or absence of other electromagnetic fields [9].

Measurements and Standards. Research Projects Laboratory has been working toward obtaining better optical property measurements such as obtaining better radiometric sources and receiver standards, participating in industry and NASA sponsored "round robins" on measurements, and obtaining specialized equipment such as a bidirectional spectroreflectometer and an in situ environmental effects chamber.

Research Projects Laboratory also participated in a series of tests carried out by the Propulsion & Vehicle Engineering Laboratory to obtain the effects of solid deposits from solids, rockets, or thermal control surfaces.

Research Projects Laboratory's portable integrating sphere spectroreflectometer (Fig. 10) was taken to the Tullahoma test site to obtain immediate measurements of optical degradation on these surfaces due to rocket plume impingement.

CONCLUSION

Research Projects Laboratory's activities in the emissivity physics areas have elucidated problems over a broad range from the theoretical and experimental research to Saturn and Saturn payload activities.

Additional experimentation in the area of thermal control surfaces (including the need for combined environmental studies and in situ measurements), is necessary to obtain a better understanding of the effects of synergism and bleaching.

In situ measurements and recovery of the Pegasus III thermal control samples would provide many answers on long-term stability in the low-earth orbit space environment of almost all important coating systems.

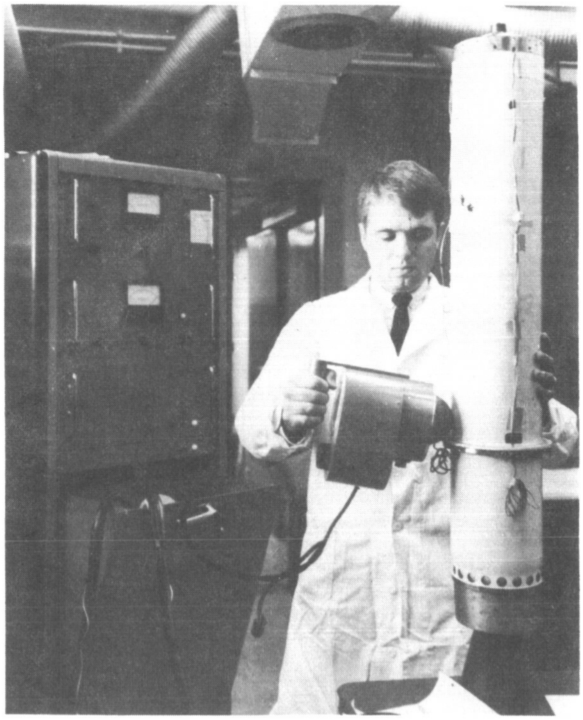

FIGURE 10. PORTABLE INTEGRATING SPHERE SPECTROREFLECTOMETER

Research Projects Laboratory is continuing many contractual and inhouse experimental efforts including the optical properties of solids (emissivity, absorptivity, transmissivity, scattering, and optical constants) and laboratory instrumentation and measurements.

REFERENCES

1. Solar Wind Damage to Spacecraft Thermal Control Surfaces. Contract No. NAS8-11269, Litton Systems, Inc., July 1965.

2. Miller, E. R.: Effect of Solar Wind Bombardment on Thermal Control Surfaces. NASA TMX-53426, April 15, 1966.

3. Calculations of the Optical Absorption of an F-Center in ZnO by Simpson's Method. Contract No. NAS8-20166, Brown Engineering TN R-172, December 1965.

4. Solar Radiation Induced Damage to Optical Properties of ZnO-type Pigments. Contract NAS8-11266, Technical Summary Report, Lockheed Missiles and Space Company, Palo Alto, Calif., June 1965.

5. Development of Space-Stable Thermal Control Coatings. Contract NAS8-5379, Report No. IITRI-U 6002-36 (Triannual Report), IIT Research Institute, Chicago, Illinois.

6. Study of Micrometeoroid Damage to Thermal Control Materials. Final Technical Report, Contract NAS8-11149, TRW No. 4146-6009-SV-000, February 1965.

7. Thermal Control Surfaces. First Annual Progress Report, Project SUPER PR-No. H-71465, July 1965.

8. Directionally Reflective Coating Study. Technical Summary Report, Contract No. NAS8-11273, Ling-Temco-Vought No. 00.603, May 1965.

9. Theoretical Study of the Radiative Emissivity of Materials. Contract NAS8-5210, PEC Corporation, Boulder, Colorado.

ULTRAVIOLET INTERACTIONS WITH SOLID MATERIALS

By

Gary M. Arnett

SUMMARY

Studies elucidating some of the major problems connected with spacecraft coating instability when exposed to solar ultraviolet irradiation are presented. The studies are concentrated on ZnO-type pigmented thermal control coatings which are among the most stable white coatings available at the present time. Basic experimental and theoretical research efforts in this area, both inhouse and on contract, are presented along with preliminary conclusions of various aspects of the program.

INTRODUCTION

Successful operation of space vehicles demands that components be maintained within their designed temperature limits. Control of temperature on an operational spacecraft is based on the exchange of radiant energy with the vehicle's environment, and therefore depends upon the optical properties of the exterior surfaces. Design requirements often dictate the use of a surface with a low ratio of solar absorptance, α_s, to the emittance, ϵ_{IR}. These surfaces are generally susceptible to damage by natural or induced radiation in space, resulting in an increase in solar absorption. The emittance is generally unaffected.

Of all sources of radiation encountered in space, both natural and induced, the ultraviolet portion, that is the 2000 to 4000 angstrom region of the solar spectrum, is the most important source of damage to surfaces with a low ratio of solar absorption to thermal emittance. For most low α_s/ϵ_{IR} surfaces, ultraviolet induced damage is at least as great as that due to other forms of radiation. In addition, all space vehicles are exposed to high fluxes of solar radiation. In contrast, not all vehicles experience high doses of Van Allen, nuclear, or other forms of high-energy radiation. Since 96.9 percent of solar radiation is between the wavelengths of 0.2 microns and 2.6 microns, the solar absorption of a material is essentially determined by its optical properties in wavelength range.

Over the past five years a large body of data on the effects of simulated solar ultraviolet radiation in vacuum on low α_s/ϵ_{IR} thermal control surfaces has been generated by various agencies concerned with spacecraft temperature control. In the past, time requirements forced efforts to be limited to accumulating relatively crude engineering design data. Available information on solar-radiation-induced damage to thermal control surfaces is almost entirely empirical. Since complete environmental simulation is never achieved in the laboratory, precise prediction of behavior in space from existing laboratory testing data is not possible. This has been illustrated by comparison of laboratory and spacecraft data [1].

The type of low α_s/ϵ_{IR} surface generally applied on spacecraft is a white coating made up of a pigment dispersed in a binder. A definitive understanding of the changes in the spectra of such systems is impossible unless the individual behavior of each component is first understood. Therefore a detailed study has been undertaken to better understand the behavior of the pigment itself. If this study is to produce positive results, it must concentrate on one pigmenting material. The ideal pigment would possess the following attributes:

(1) Simple, well-defined chemical and electronic structure

(2) Data available on the optical, electrical and related physical properties

(3) Representative of a class of stable white pigments

(4) In use in promising thermal control coatings.

Zinc oxide possesses each of the above characteristics to a greater degree than any other single material. ZnO, when used as a pigment with a methyl silicone or potassium silicate binder is one of the most ultraviolet-stable thermal control coatings available. Furthermore, its properties are similar to those of titanium dioxide, zinc sulfide and stannic oxide, which are used as pigments in promising white thermal control surfaces. From this information it was decided that the study of ZnO would provide a logical starting point for investigation of the mechanisms involved in solar-radiation-induced damage to low α_s/ϵ_{IR} surfaces.

Research Projects Laboratory has approached this theoretical and experimental research problem with both inhouse investigations and on contract with Lockheed Missiles and Space Company's Research Laboratories. The studies have been directed toward identifying the primary mechanisms involved in solar-radiation-induced damage to the optical properties of ZnO-type semiconductor pigments, as exemplified by ZnO itself. Knowledge of the damage mechanism will greatly simplify the problem by providing a rational basis both for the design of environmental tests and for interpretation of the resulting data. Ultimately, it is hoped that such knowledge will guide material specialists in the development of optimum materials for thermal control purposes.

The work reported under the contractual portion of this paper was conducted at Lockheed Missiles and Space Company's Research Laboratories, Palo Alto, California, under the direction of Mr. L. A. McKellar and Dr. S. A. Greenberg (Contract NAS8-11266). The inhouse portion was conducted in the laboratories of Research Projects Laboratory, Marshall Space Flight Center.

CONTRACTUAL EFFORTS

The work conducted on the previously mentioned contract can be summarized by the following studies: (1) optical transmission and reflectance studies, (2) in situ bidirectional studies, (3) photoconductivity measurements, and (4) theoretical band structure studies. Discussed below will be typical results obtained under each of the four major areas of effort.

Figure 1 shows a typical radiation test of the spectral reflectance of particulate ZnO before and after ultraviolet irradiation in vacuum. One of the most interesting features of this type of study is the comparison of the optical properties exhibited by samples that had identical irradiation times of 860 sun-hours. One was measured within one hour after irradiation and the other was exposed to atmospheric conditions for 120 hours before measurements were performed. The 120-hour time-lapse measurement demonstrates considerable bleaching throughout the spectrum. The sample irradiated for 950 sun-hours (nearly 100 sun-hours longer than the other cases) and measured just under two hours after exposure to atmospheric conditions, appeared to have less damage than the sample irradiated for 860 sun-hours that was measured within one hour after exposure to the atmosphere. Here one sun-hour is defined as the

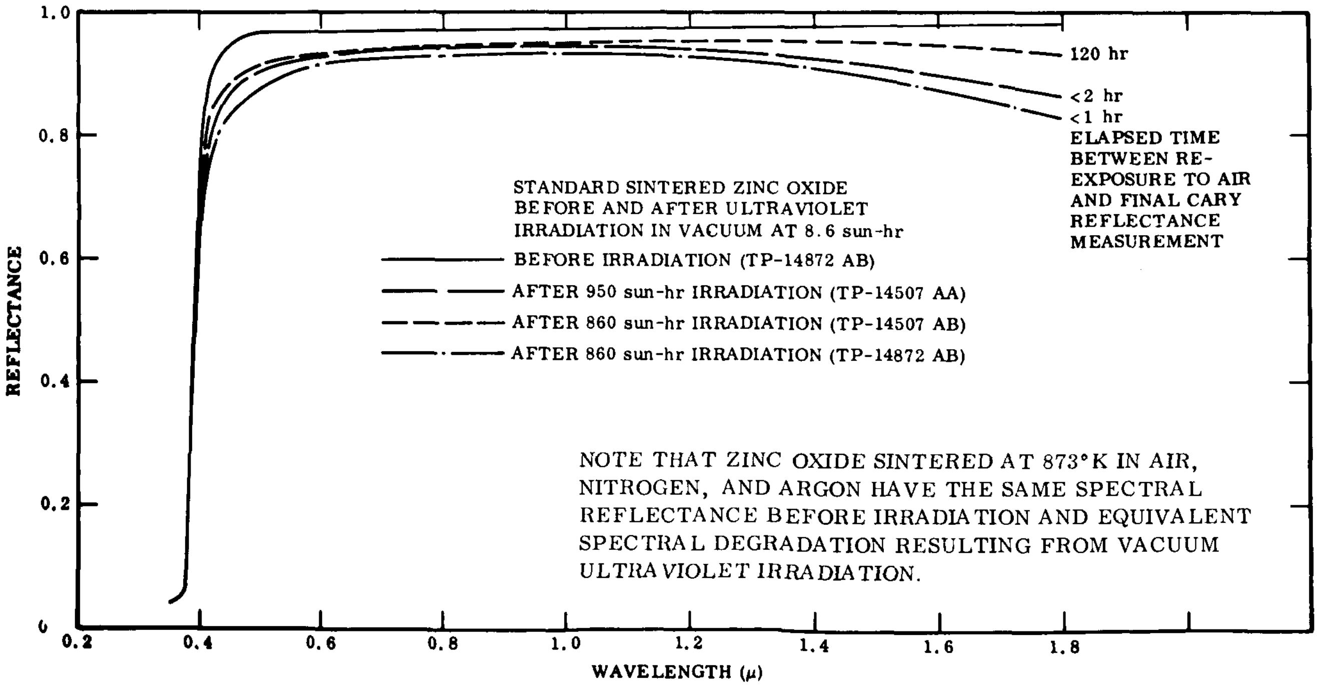

FIGURE 1. SPECTRAL REFLECTANCE OF PARTICULATE ZnO BEFORE AND AFTER UV IRRADIATION IN VACUUM

amount of irradiation incident upon a sample in outer space at one astronomical unit from the sun in the region of 2000 to 4000 angstroms. It should also be noted in this figure that little, if any, shift in the band edge can be detected for samples measured in this manner. Results such as these indicate that at least some of the induced damage is not permanent but is subject to bleaching. For true measurements of the induced damage, such as that encountered in outer space, samples must be measured while still in their irradiation environment. This study led to the development of what Lockheed calls their "in situ bidirectional reflectance device." Spectral results received from this device are normalized around 6000 angstroms measurement as obtained from their integrating sphere. Thus the instrument has proven to be a good and accurate device for making in situ reflectance or transmission measurements. Figure 2 demonstrates results obtained from this instrument. The before-irradiation curve is not shown in this figure, but would be identical to the unirradiated curve in Figure 1. In Figure 2 the edge of the absorption band has moved out into the visible region after only 52 hours of irradiation. Sometime after terminating the irradiation and before allowing the pressure to rise within the vacuum chamber, the edge of the absorption band is recovered. It should be noted in Figure 2 that the initial bidirectional measurement was taken 20 minutes before termination of irradiation and the next measurement was taken 5 ½ hours before allowing the pressure to rise 10.68 newtons per square meter (80 microns). It has been demonstrated that if the pressure is allowed to come to a somewhat higher value of 66.7 to 133.3 newtons per square meter (500 to 1000 microns), the recovery is instantaneous, especially in the infrared region, but as can be seen, is not happening at a pressure of 10.68 newtons per square meter (80 microns).

Figure 3 shows the spectral dependence of optical absorption and photoconductivity. These studies have been performed to obtain information on the recombination and trapping states that bear directly on the degradation mechanism, and also to lay the groundwork for the use of the photoconductivity technique in investigating defects produced in degraded single crystals. The first point to note on the optical absorption data is the apparent shift of ~ 0.04 electron volts of the fundamental absorption edge to low energy with the Li addition (Li doping reduces the number of electron charge carriers). This shift is either the result of a high density of shallow acceptor states or a deformation of the lattice itself caused by the high impurity concentration. The absorption data do not go to high enough values of the absorption coefficient to resolve this point.

The measurements of the spectral dependence of the photoconductivity were carried out at room temperature in air on the Li-doped crystal. Radiation from a Zenon compact arc source was passed through

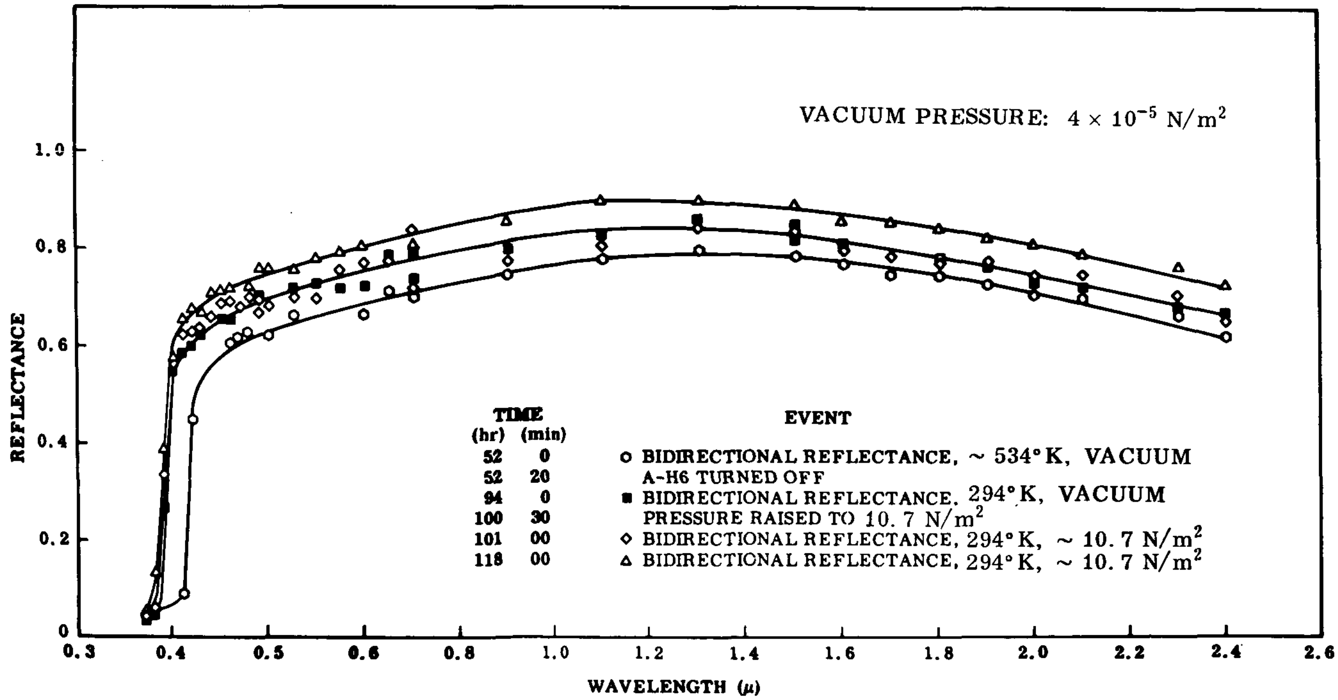

FIGURE 2. RECOVERY OF UNPRESSED, UNSINTERED ZnO AT 294° K

a Perkin-Elmer 112 monochromator and then brought to focus on the sample. The chopping frequency of 1 kilocycle was chosen to insure that only the fast photoconductive process was being observed. Figure 3 compares the photoconductive response and the absorption edge data on the Li-doped sample. The essential feature is that the photoconductivity observed is a bulk as opposed to a surface phenomenon,

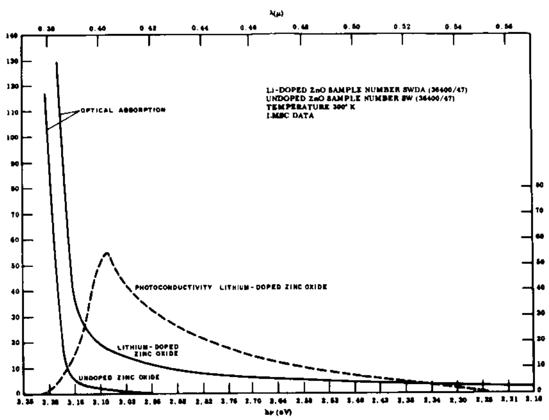

FIGURE 3. SPECTRAL DEPENDENCE OF OPTICAL ABSORPTION AND PHOTOCONDUCTIVITY

which is supported by the following arguments. The photoconductive signal decreases as the absorption coefficient increases sharply because of the band-to-band absorption that is the fundamental band edge. The sample surface was purposely not etched, thus providing a surface with a high recombination rate. Therefore in these experiments, radiation which is absorbed very close to the surface (that results from a high absorption coefficient) does not give rise to a photoconductive signal. The next feature to note is that the signal peaks at the wavelength for which the absorption coefficient corresponds approximately (order of magnitude) to the reciprocal of the sample thickness or ~ 0. 04 centimeters. At longer wavelengths an increasing amount of the incident energy is transmitted through the sample because of the decreasing absorption coefficient. The photoconductive responses decrease proportionately.

The results of the photoconductivity studies lend strength to the bulk impurity state model used in the theoretical studies. Figure 4 shows this impurity model with the band-gap energy at 3. 2 electron volts, which corresponds to 0. 38 microns.

To round out the theoretical portion of the first phase of this program, it was felt that a thorough

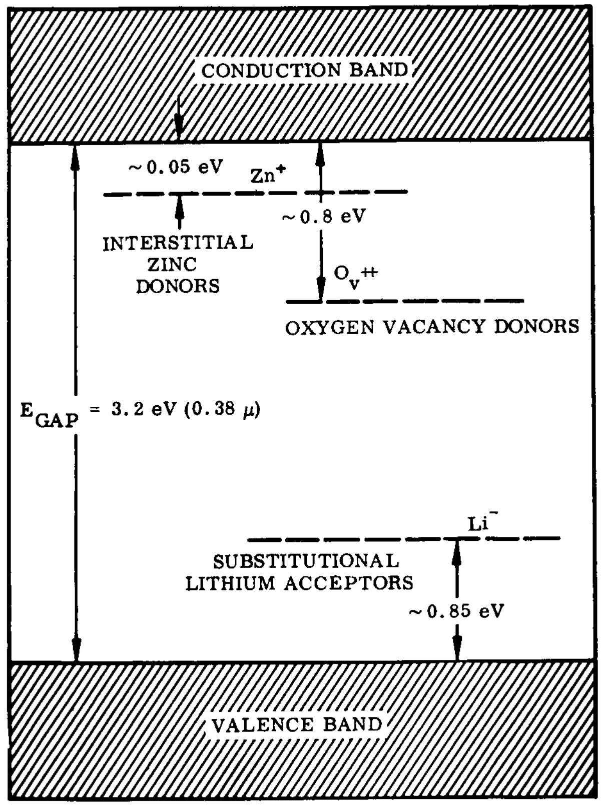

FIGURE 4. BULK IMPURITY STATES

understanding of the electronic energy band structure of a crystal was a necessary prerequisite for the detailed interpretation of many important transport and optical properties. Therefore, theoretical band structure studies of ZnO were initiated to complement the experimental program. To the best of our knowledge, no serious attempt has previously been made to elucidate the electronic band structure of ZnO. Therefore, our efforts in this area should be both useful and unique.

After detailed consideration of the chemical, electronic, and physical structure of ZnS and ZnO, it was determined that the band structure calculations could best be accomplished by utilizing the "method of corresponding states," with ZnS calculations being the basis for work carried out on ZnO. Thus the reliability of the ZnO results cannot be any better than the ZnS calculations that were carried out by Herman and Skillman using the orthogonalized-plane-wave method. An energy band model was derived for ZnO from these calculations, which are too detailed and complex to discuss in this paper (for further information on these calculations, see contract report mentioned in acknowledgements). The plausibility of the desired model was then tested by the method of weak binding (the nearly free electron model) and by the method of tight binding. These tests indicated that the derived band structure for ZnO was probably a good first estimate [2]. Further work in this area may prove to be quite valuable because of the crucial role that the energy band structure can play in estimating the energy levels of both surface states and bulk impurity states.

INHOUSE EFFORTS

The Space Thermodynamics Branch of Research Projects Laboratory at Marshall Space Flight Center is conducting inhouse experimental and theoretical studies on the interaction of electromagnetic radiation with solid state matter. The major parts of the inhouse efforts can be outlined as follows: (1) ultraviolet irradiation parameter studies, (2) electrical conductivity studies, (2) optical absorption studies, (4) magnetic susceptibility studies, and (5) electron paramagnetic resonance studies. Figure 5 shows the main ultraviolet irradiation facility. Early in the program the use of a diffusion-pumped vacuum system was discontinued because oil contaminated the ZnO-type materials; therefore, a sorption-rough and ion-fine pumping system is now used to keep contamination to a minimum. A residual gas analyzer was placed within the system as a permanent fixture (not shown in figure). This will allow the experimenter to study the partial pressure of the gases evolving from the sample material during ultraviolet irradiation. After conducting studies of the intensity versus time of the high-pressure mercury arc lamps used as the ultraviolet irradiation source, it became evident that some type of intensity control was needed to compensate for the erratic behavior of the lamp. The control on the left and the housing on top of the irradiation chamber provide (through a series of servomechanisms) a constant intensity of irradiation upon the sample. The system allows the experimenter to readily choose the intensity, or during irradiation, change the intensity of irradiation upon the sample, with continuous recording of intensity and irradiation time. The intensity-monitoring device is an Eppley thermopile which can be filtered with a selection of eight different filters located on a filter wheel, with the position of interest selected on the control console.

FIGURE 5. UV IRRADIATION FACILITY

The specific study being conducted using the apparatus shown in Figure 5 is the effect of ultraviolet irradiation on the electrical conductivity of ZnO single crystals [3]. The irradiation was filtered using a Corning CS7-37 filter so that the principal illuminating wavelengths were concentrated about 3650 angstroms, which is equal to or greater than the band gap energy in ZnO. The sample was irradiated for 50 hours at 0.013 watt per square centimeter and Table I shows the results obtained. The observed increase in conductivity after 50 hours of irradiation may result from

TABLE I. RESULTS OF ELECTRICAL RESISTIVITY STUDIES

	Time (min) after Potential is Applied			
Electrical conductivity in $ohm^{-1}cm^{-1}$	0	4	8	10
Before irradiation in air	5.50×10^{-3}			4.685×10^{-3}
After irradiation in vacuum	7.127×10^{-3}	9.528×10^{-3}	1.003×10^{-2}	1.003×10^{-2}
After irradiation and letting air in vacuum chamber	4.685×10^{-3}	4.78×10^{-3}	4.499×10^{-3}	4.499×10^{-3}

the loss of oxygen from the sample, while the excess zinc atoms become ionized and diffuse into interstitial positions in the lattice, which accommodates them. The oxygen evolved has little chance of being reabsorbed by the crystal because of the vacuum environment of approximately 5.34×10^{-5} newtons per square meter (4×10^{-7} torr). Electrons which make possible the electric conduction are removed from the zinc and compared in a similar way with thermal excitation, as reported by Scharowsky. The increase in the conductivity of the crystal implies that the zinc atoms are not electrically neutral. However, lowering the conductivity by allowing air to enter the vacuum chamber is an indication that current strength is decreased by oxygen presssure and the chemisorption of oxygen. It seems probable that the effect of heating may be comparable with the effect of ultraviolet irradiation, but no definite conclusion can yet be drawn. It is hoped that the bleaching of the resistivity noticed in these data can be correlated with the optical bleaching data which were obtained under similiar circumstances.

Figure 6 shows data received from inhouse optical absorption studies.* The ZnO crystal disc

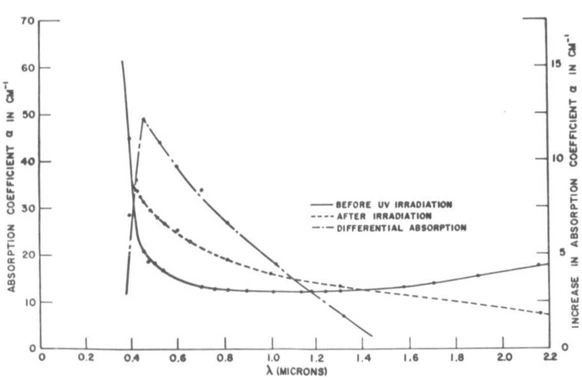

FIGURE 6. OPTICAL ABSORPTION IN ZnO SINGLE CRYSTAL OF THICKNESS 0.21539 mm AT 300°K

used here was subjected to similar irradiation parameters as mentioned in the previous study. The absorption measurements were not made in situ, but the measurements made are a good indication of the permanent bulk damage induced by the ultraviolet irradiation. Of special interest is the recovery of the sample in the infrared such that the absorption coefficient is less after irradiation and bleaching than before irradiation. This phenomenon cannot be adequately explained at this time.

ZnO displays basically diamagnetic properties; the susceptibility of ZnO becomes less and less diamagnetic with ultraviolet irradiation, which demonstrates the paramagnetic nature of the induced damage sites.

Figure 7 shows a portion of the magnetic susceptibility equipment being utilized to study magnetic properties of ZnO before, after, and during ultraviolet exposure. The microbalance shown at the top of Figure 7 is operated along with the electromagnet

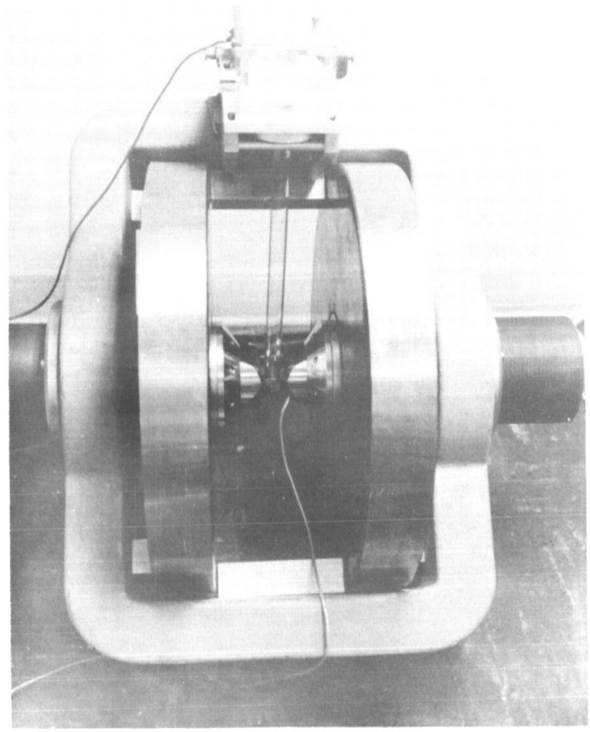

FIGURE 7. ELECTROMAGNET WITH MICROBALANCE

at a distance of six feet or greater to reduce disturbances when making precise measurements. Measurements are taken at the same distance with the help of a lamp and scale arrangement and a counterbalancing coil mounted on the center of the beam arm which is supported by a small quartz fiber.

* Lal, R. B.; and Miller, E. R.: "Effect of Ultraviolet Irradiation on Fundamental Optical Absorption in ZnO Single Crystals" (to be published later).

Inhouse studies are also being conducted on the absolute spin concentration, g-value measurements, and the spin-spin and spin-lattice relaxation time using an electron paramagnetic resonance apparatus shown in Figure 8. In this figure, the ultraviolet radiation source, used in irradiating the ZnO particulate or single crystal samples, is being placed between the pole-tips of the magnet. ZnO displays no resonance absorption before irradiation. Because of the bleaching phenomenon observed, the irradiation must be conducted while measurements are being taken. When the density of the unpaired electrons, or paramagnetic centers, increase into the sensitivity range of the instrument, resonance absorption is recorded. The instrument has the dual sample cavity capability so that resonance spectra can be directly compared to a calibrated sample. Thus far, observations have been made of the resonance spectra and the instantaneous bleaching when irradiation is terminated. Precise g-value or Landau factor measurements are presently being conducted along with detailed studies of the relaxation phenomena.

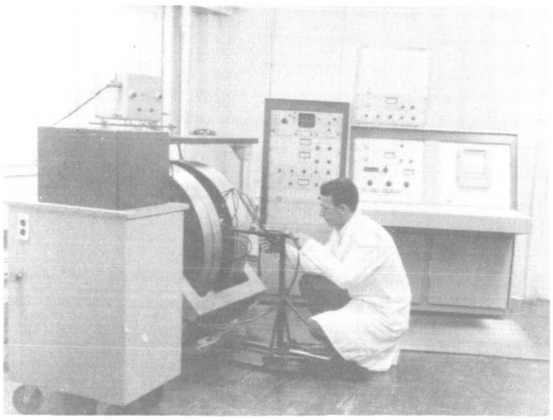

FIGURE 8. INSTRUMENT FOR MEASURING ELECTRON PARAMAGNETIC RESONANCE ABSORPTION

Figure 9 shows the X-ray spectrometer used in making detailed impurity concentration measurements on all samples of ZnO before basic magnetic or optical absorption studies are conducted.

CONCLUSION

The program has proceeded to the point where a preliminary model of the ultraviolet-induced damage mechanism can be formulated, although there are many unanswered questions. Throughout the course of the experimental studies, one unifying trend in the data has been apparent - many of the changes in the optical properties of zinc oxide appear in part to be connected with the photoadsorption and desorption of oxygen by the crystal.

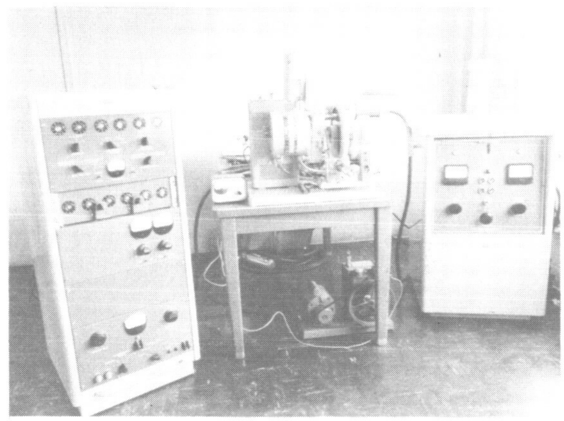

FIGURE 9. X-RAY SPECTROMETER

REFERENCES

1. Neel, C. B.: Research on the Stability of Thermal-Control Coatings for Spacecraft. NASA TMX-51196, October 1963.

2. Lockheed Missiles and Space Company, Technical Summary Report, Contract No. NAS8-11266, June 27, 1964 - June 27, 1965.

3. Lal, R. B.; and Arnett, G. M.: Nature, 208, 1305.

PEGASUS THERMAL EXPERIMENTAL RESULTS

By

William C. Snoddy

N67-24646

SUMMARY

Results thus far obtained from the analysis of Pegasus orbital thermal data indicate that the temperature of the on-board electronics for all three Pegasus spacecraft is being maintained within the desired range in spite of an overheating of the S-IV stage and the service module adaptor. The S-IV stage and the service module adaptor were designed to act as heat sinks for the electronics. At this time it is believed that the overheating was caused by a degradation of the optical characteristics of the paint applied to these areas. This degradation is presumed to have resulted from damage caused by plume impingement from the retrorockets on the booster during stage separation and from the rocket used to jettison the Apollo escape tower. The successful operation of the thermal louvers attached to the electronics canister is credited with maintaining the proper thermal environment even though these difficulties were encountered.

Results from an "environmental effect sensor package" indicate a space-environment-induced degradation of several thermal control coatings. Some of these supposedly "space-stable" coatings have had a 100 percent increase in their solar absorptance to infrared emittance ratio. Results from these sensors are also used to study the earth's albedo. The albedo has been found to vary greatly and results are now being correlated to weather photographs.

INTRODUCTION

The first Pegasus spacecraft was placed in orbit on February 16, 1965 followed by a second one on May 25, 1965 and the final one on July 30, 1965. The primary objective of this series of satellites is the further definition of the meteoroid hazard to manned space flights. In addition to telemetering data regarding the meteoroid environment, each of the spacecraft has transmitted many millions of bits of thermal information. These thermal data are being evaluated inhouse at Marshall Space Flight Center; a discussion of some of the results obtained thus far follows.

EVALUATION OF THERMAL DESIGN OF LARGE AREAS

Two sections of the Pegasus spacecraft represent the largest, inflexible surface of any satellite ever placed in orbit having a lifetime of more than a year. These are the meteoroid detector panels with 200 square meters of surface and the S-IV stage together with the service module adapter having a total of about 300 square meters of exterior surface (Fig. 1).

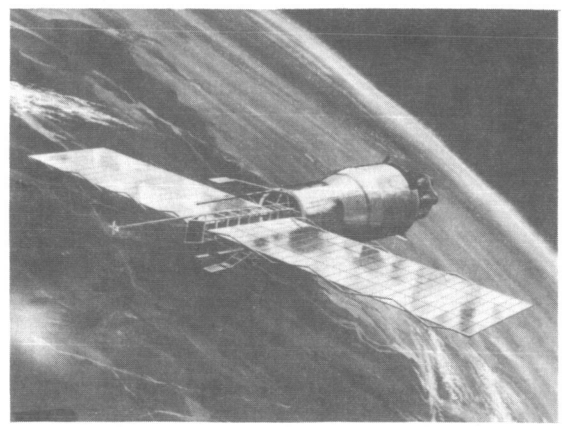

FIGURE 1. PEGASUS SATELLITE

In the case of the detector panels, the initial question to be answered by thermal data analysis was whether the temperature of the panels with their coating of MTL-3 Alodine remained within the design range of 165° to 395°K. Some typical data from Pegasus I are shown in Figure 2 and indicate a maximum temperature of about 350°K with a minimum of 225°K. The top curve in Figure 2 represents the temperature of the side of the detector panels facing the sun; the bottom curve represents the temperature for the side away from the sun. The large variations are caused by passage of the satellite through the earth's shadow. Continuous monitoring of these temperature probes indicates that these values represent near extremes. Therefore, the temperatures of the detector panels on Pegasus I as well as the other Pegasus

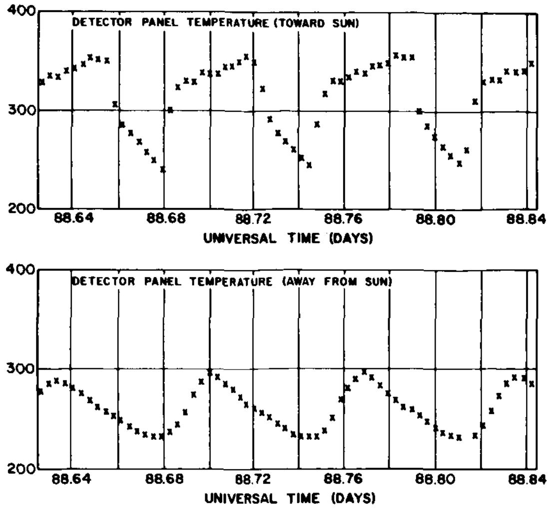

FIGURE 2. PEGASUS I DETECTOR PANEL TEMPERATURE VARIATION

satellites have thus far remained well within the design range.

The temperature of the service module adapter at the top of the S-IV stage has been 20° to 30°K warmer than expected throughout the lifetime of all three Pegasus satellites. Since this area, together with the S-IV stage, is used as a radiative heat sink by the Pegasus electronics, such an increase in temperature has a direct bearing on their temperatures. The cause of these warmer temperatures is apparently the result of a higher than expected ratio of solar absorptance (α_s) to infrared emittance (ϵ_t) of the exterior surface. The surface in this case was a zinc-oxide pigmented methyl silicone paint (designated S-13). The expected α_s/ϵ_t value for this paint was 0.22 and this was the value measured by personnel from the R-RP-T laboratory on the pad a few days before launch. However, detailed analysis of the telemetered thermal data indicates an orbital value of α_s/ϵ_t of about 0.5, an increase factor of two or more (Fig. 3). Part of this increase can be explained by the unexpected degradation by ultraviolet radiation of S-13 discussed earlier in this review by E. Miller and G. Arnett. The rest of the increase seems most likely to have been caused by contamination of the paint by plume impingement from the retrorockets during booster separation and subsequent solar ultraviolet degradation. It is well known that S-13 is

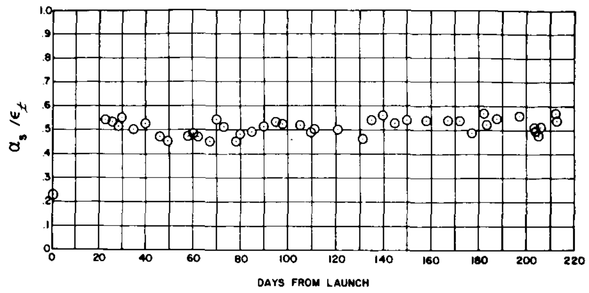

FIGURE 3. S-13 COATING DEGRADATION ON THE PEGASUS I SMA

stable to ultraviolet radiation only so long as it is exceptionally clean. Thus, all of the degradation that might have taken years, if ever, to occur took place apparently during the first few days or perhaps even hours in orbit. The gap in the data for the first 20 days (Fig. 3) was caused by difficulties in analysis resulting from complex altitude variations.

ELECTRONIC CANISTER TEMPERATURES AND LOUVER OPERATION

The electronics of the Pegasus spacecraft are located mainly in a canister inside the payload adapter (service module adapter) at the bottom of the center section structure (Figs. 4 and 5). During flight the top and side of this canister are covered with superinsulation to prevent heat losses. A louver assembly attached to the bottom of the canister (Figs. 5 and 6) is designed to furnish automatic radiative coupling with the service module adapter and the S-IV stage which act as heat sinks. Each louver blade is driven by a bimetallic strip such that the louvers normally remain closed. However, a rise in canister temperature will cause the louvers to open allowing the excess heat to be lost by radiation. The main point of concern with the operation of the louvers was the requirement for long lifetime (18 months) reliability. By indirect methods utilizing telemetered temperature and spacecraft orientation data the apparent average opening angle of the louver blades was determined for several times during the first eight months in orbit for Pegasus I (Fig. 7). The points shown in Figure 7 are representative of a great number of similarly generated data points. This analysis has shown that the louvers appear to be performing successfully. The higher than expected temperature of the service module adapter (SMA) and the S-IV stage is apparent by the fact that the louvers never appeared

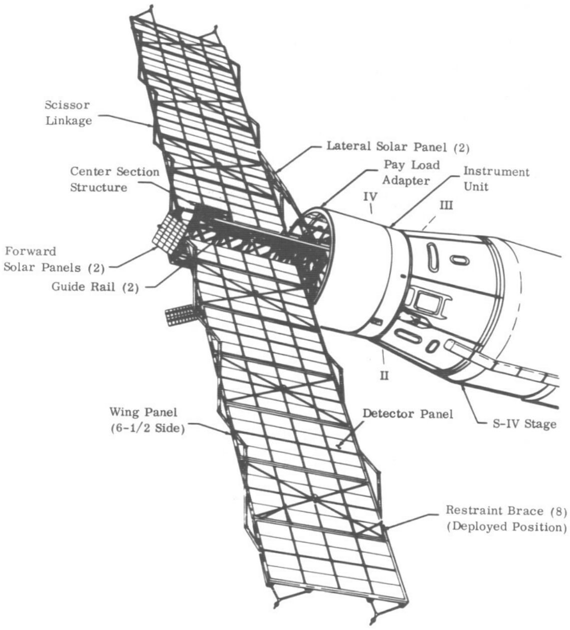

FIGURE 4. MICROMETEOROID MEASURING CAPSULE

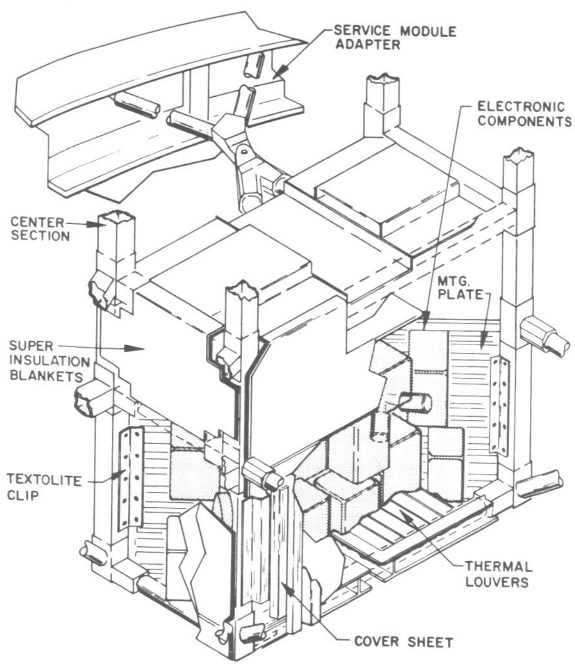

FIGURE 5. ELECTRONICS CANISTER

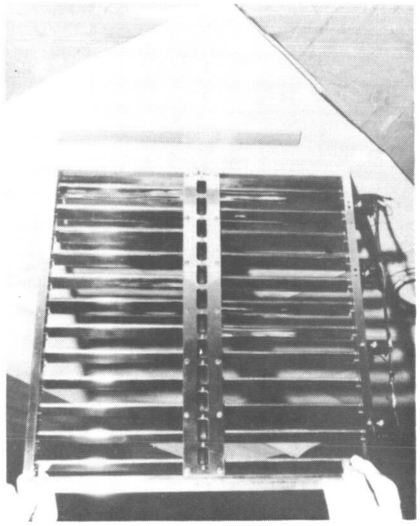

FIGURE 6. LOUVER ASSEMBLY

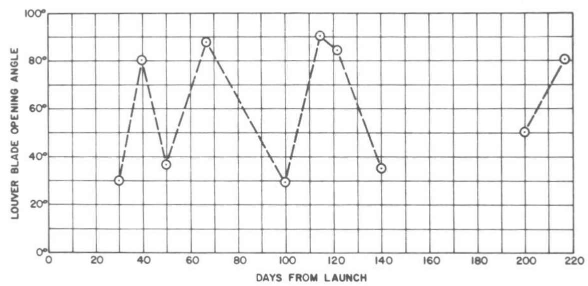

FIGURE 7. LOUVER ACTIVITY, PEGASUS I

to be fully closed even though the original design was such that they were to remain closed almost 90 percent of the time. Thus, without an active system such as the louvers, serious thermal problems could have resulted from these higher sink temperatures.

How well the louvers have compensated for external thermal variations is apparent by the behavior of a representative canister temperature such as an internal battery temperature (Fig. 8). During the first 290 days of Pegasus I's lifetime this temperature reached a maximum of 305°K and a minimum of 293°K. After this time there was approximately a 10°K rise in temperature which has been traced to a failure in an external zener-diode package.

ENVIRONMENTAL EFFECT SENSORS

Also flown on each of the Pegasus spacecraft was a small sensor package composed of four thermally

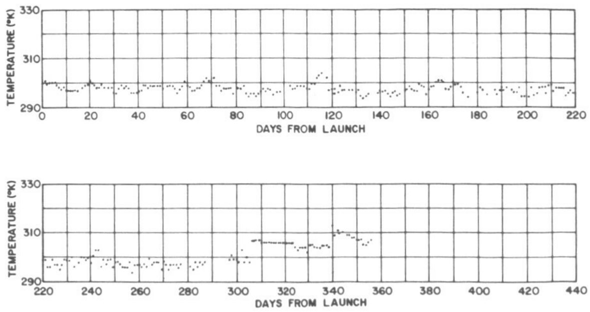

FIGURE 8. INTERNAL BATTERY TEMPERATURE, PEGASUS I

isolated discs (Figs. 9 and 10). The discs are mounted such that they have a two-pi steradian view of space and the temperature of each is stored and telemetered upon command. A different thermal control coating is applied to each disc, and by knowing their temperatures and the satellite's altitude the radiometric characteristics of these coatings as a function of time in space can be determined. Such a

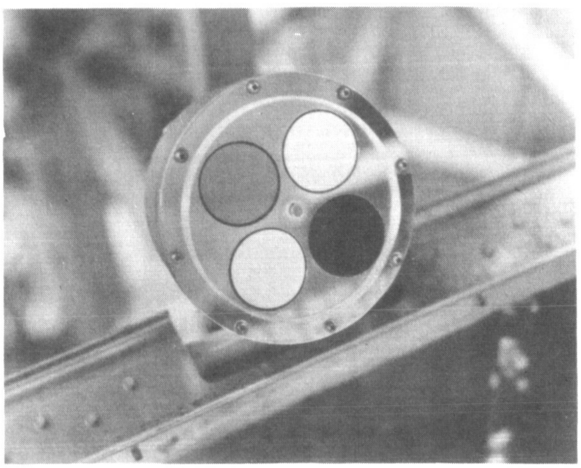

FIGURE 9. SENSOR PACKAGE WITH FOUR DISCS

determination for the sensor on Pegasus I gave the results shown in Figure 11. The initial sharp rise in α_s / ϵ_t for both the S-13 and rutile paints is apparently the same increase recently measured in the lab and discussed earlier in this review. It should be pointed out that this sensor as well as the entire Pegasus spacecraft was covered by a dummy Apollo spacecraft during ascent, and thus was not exposed to the retrorocket plume discussed previously in connection with the degradation of the S-13 on the

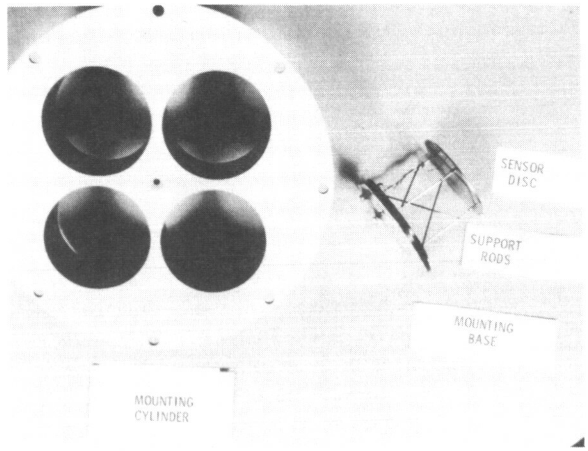

FIGURE 10. COMPONENTS OF SENSOR PACKAGE

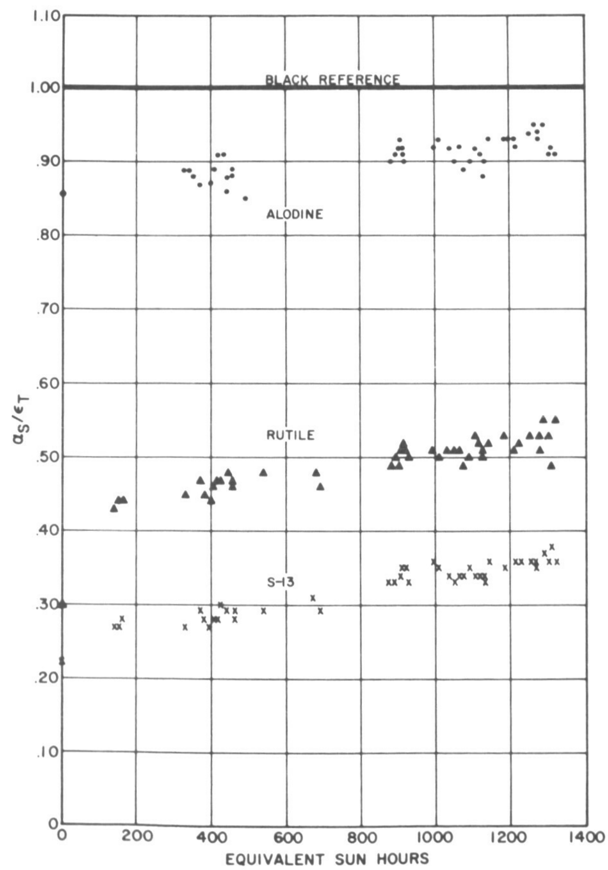

(Initial Values of α_s / ϵ_t Based on Pre Launch Lab Measurements)

FIGURE 11. PEGASUS I ENVIRONMENTAL EFFECT SENSOR DATA

S-IV stage. Still the amount of degradation shown by this protected "space-stable" S-13 paint on the environment effect sensor indicates the nature of the problem faced by the thermal engineer in the selection of thermal control coatings. In many applications a degradation in this amount is sufficient to cause a 30° to 40°K rise in temperature which could lead to a catastrophic failure.

Once the radiometric characteristics of the disc have been ascertained, it is possible to measure the earth albedo flux during the times the sensor faces the earth. Preliminary efforts have given the results shown in Figure 12, where the effective earth albedo is plotted as a function of position in orbit. The "effective earth albedo" is the same as the Bond* albedo assuming a diffuse earth with homogeneous reflectance characteristics. However, it should be noted that the measurements themselves indicate the inhomogeneous characteristic of the earth's surface. Thus, the determination of a "Bond albedo" is useful for comparison purposes only. These data are now being analyzed with the aid of Tiros and Essa photographs in an attempt to correlate cloud cover and terrain conditions with the measured results.

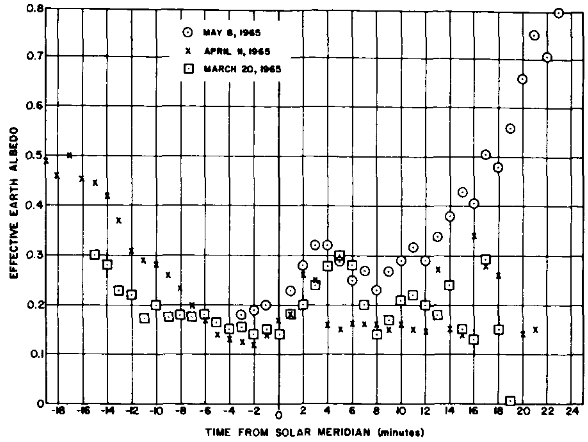

FIGURE 12. PEGASUS I ALBEDO MEASUREMENTS

CONCLUSION

In conclusion, it is noted that the analysis of Pegasus thermal data has, thus far, resulted in extremely worthwhile results. It is anticipated that these results will be further amplified as these studies continue. Such studies will include a comparison of results between Pegasus I, II, and III; a correlation of albedo measurements with cloud cover and theoretically predicted Rayleigh scattering; and the continuation of thermal coating degradation analysis.

* Bond albedo is the ratio of the total light energy reflected from a planet to the total light energy incident.

RESEARCH IN INSTRUMENTATION FOR RADIOMETRY AND SPECTROMETRY

By

Harlan D. Burke

N67-24647

SUMMARY

Infrared measuring systems typical of those flown on the Saturn vehicles are discussed. These systems are used to detect fires in the vehicle and to determine spectral characteristics of the exhaust plume, heat flux to the heat shield from the hot gases in the exhaust, and heat flux to other vehicle structures from aerodynamic forces during ascent. The principle of operation and typical parameters of each type of instrument are discussed.

INTRODUCTION

Infrared measurements on the Saturn vehicles are concerned with determining the spectral characteristics of the plume and the convective, radiative, and total heat fluxes incident to the heat shield from the hot gases in the engine exhausts, and the heat flux to other vehicle structures as a result of the aerodynamic forces encountered during ascent. Extensive wind tunnel tests on scale models and captive test firings have permitted the thermal design of systems to theoretically approximate the heating rates obtained during flight. Actual flight data are used to correlate the effectiveness of the test programs leading to the thermal design of the vehicle parameters. The complexity of the problems of heat flux analysis has required the research and development of highly specialized radiometer and spectrometer instrumentation systems for flight measurements.

The infrared and heating rate measuring devices and systems used in the Saturn program have changed with technology and as confidence in the techniques was established. The instruments used by MSFC are the integrated and direct reading radiometers, color wheel radiometers, infrared spectrometers, and special systems such as those used in fire detectors. No one instrument will provide all the data required for complete thermal analysis of heating rates obtained during flight. This discussion will briefly describe the features of each system and illustrate design techniques.

INTEGRATING RADIOMETERS

These instruments are ideally suited for measurement of total heat flux over a period of time. Rapidly fluctuating heating rates are not recorded and time-of-flight data are obtained only through time-consuming analysis of the radiometer data and the environmental conditions. Many types of radiometers are used in space vehicle instrumentation programs. The slope calorimeter has been most frequently used by MSFC. Its principle of operation is that given any thermally isolated mass of known dimensions and thermal properties, it is possible to solve for the heating rate to which it has been exposed by knowing its temperature versus time history. Thermal isolation of the mass minimizes conduction losses to the mounting wall. While it is possible to reduce these losses, there are conduction losses inherent to each design. These losses can be determined accurately and individual calibration curves can be established.

The radiometer as shown in Figure 1 (a) measures the total convective and radiant energy incident to its surface. Radiant energy only is measured by the radiometer shown in Figure 1 (b). The convective component is prevented from reaching the radiometer sensing surface by a lens system. The lens material in this instrument can be selected to permit transmission in spectral ranges of particular interest. Sapphire and quartz have been the primary filter materials used by MSFC because the radiation to be measured is almost entirely within the 0.2- to 5-micron region.

Figure 1 (c) shows a typical equation used to obtain the heating rate data to the sensor. When the total energy absorbed by the radiometer is desired, the equation

$$\int_{t=t_o}^{t} q\,dt$$

would be applicable. Theoretical analysis of the flight data is accomplished by comparing the temperature as a function of time curves, shown in Figure 2 (a), with the heat flux as a function of rate of change of temperature with time curves, shown in

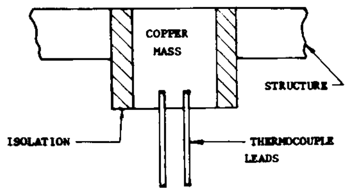

(a) TOTAL

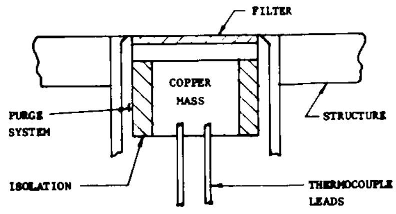

(b) RADIANT

(c) HEAT FLUX EQUATION

$$\dot{q} = \rho C_p L \frac{dT}{dt} + K(T - T_o) + \epsilon \sigma T^4$$

Where:

$\dot{q}$ = Absorbed Heat Flux

ρ = Mass Density of Slug

C_p = Specific Heat of Slug

L = Slug Thickness

T = Slug Temperature

T_o = Initial Slug Temperature

ϵ = Emissivity

t = Time

K = Loss Constant

σ = Stephan-Boltzmann Constant

FIGURE 1. TYPICAL SLOPE RADIOMETER

Figure 2 (b). Experimental analysis of the integrated flight data is accomplished by programming a heat flux into a simulated flight radiometer installation to exactly reproduce the flight data. This programmed heat flux is then observed with a standard heating rate radiometer. The theoretical and experimental analyses reduce the integrated flight data (shown in Figure 2d as integrated flight data) as a function of temperature and time, to incident heat flux as a function of time as shown in Figure 2 (d).

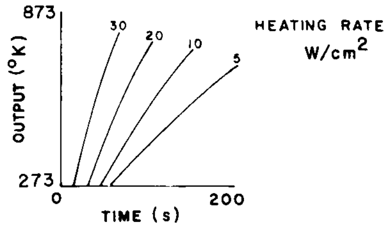

(a) EXPOSURE TIME VS SLUG TEMPERATURE

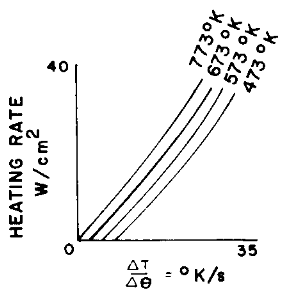

(b) CALIBRATION CURVE

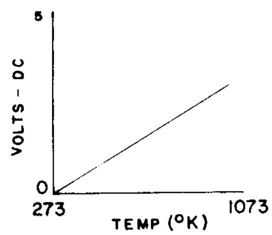

(c) AMPLIFIER CALIBRATION

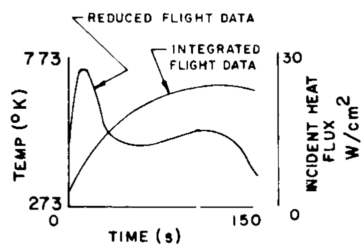

(d) RAW FLIGHT DATA VS REDUCED FLIGHT DATA

FIGURE 2. CALIBRATION AND DATA CURVES FOR SLOPE RADIOMETER

DIRECT READING RADIOMETER

The outputs of direct reading radiometers are directly proportional to the incident heating rates. Fast response and recovery times can be designed into the detector system to permit measurement of transient heating rates. These features minimize the time required for calibration and data reduction. The asymptotic or membrane calorimeter is the most advanced instrument for flight measurements. This type of heating rate sensor is different from the slope or integrated radiometer in that its output is proportional to the temperature gradient between the center of a thin constantan disc and its periphery. This temperature gradient is directly proportional to the heating rate. Figure 3 illustrates the basic design of the sensor and the equation that expresses the relationship between the heating rate and output signal. This dependence of $\dot{Q}$ on ΔT could indicate a

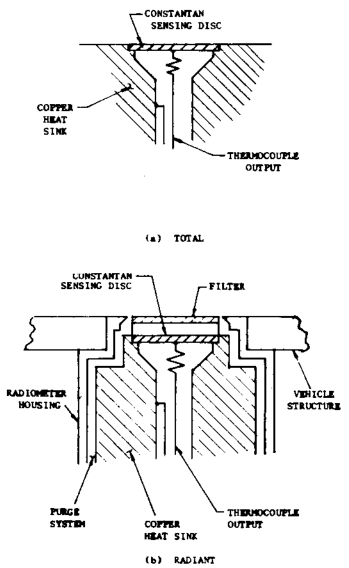

(c) HEATING RATE EQUATION

$$\dot{Q} = 4.52 \frac{SK}{R^2} \Delta T$$

Where:

$\dot{Q}$ = Heating Rate in Watts/cm^2

S = Sensor Thickness

K = Sensor Thermal Conductivity

R = Radius of Active Sensor

ΔT = Temperature Differential

FIGURE 3. TYPICAL DIRECT OUTPUT RADIOMETER

nonlinearity if the thermal EMF curve of the temperature sensor is not linear. In practice, the conductivity K changes with temperature in the opposite direction by approximately the same ratio. Figure 4 shows typical calibration curves and flight data.

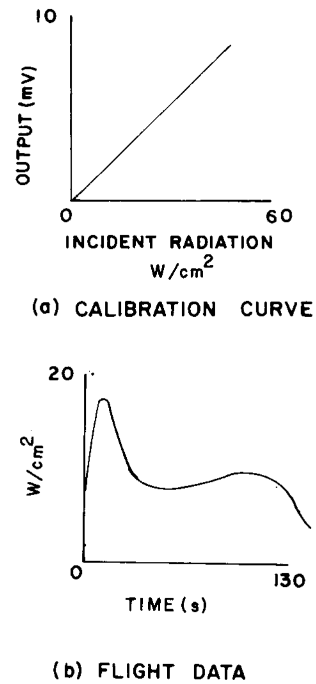

FIGURE 4. CALIBRATION AND DATA CURVES FOR DIRECT OUTPUT RADIOMETER

COLOR WHEEL RADIOMETER

The color wheel radiometer was developed for MSFC by Minneapolis Honeywell under contract NAS8-5099. It is a rapid scan spectral radiometer operating in the infrared spectrum from 2 to 5 microns with ten separate spectral bands. The system is normally used to measure the spectral distribution of rocket plumes but can be modified to measure any selected bands for which filters are available. The radiometer has been flight qualified to the Saturn IB environmental requirements. The block diagram of the radiometer is shown in Figure 5. The design features (1) an 11.4-centimeter (4.5-inch)-diameter Dall-Kirkham optical system with a clear aperture of 77.4 square centimeters (12 square inches) and a field of view at 50 percent transmission of 3.2 milliradians in the Z axis and 4.6 milliradians in the Y axis, (2) a germanium window that allows the passage of infrared radiation, but seals the radiometer against the entrance of dust, (3) a rotating filter wheel turning at approximately three revolutions per second containing ten spectral filters, (4) a radiation chopper wheel that modulates the incoming radiation at a frequency of 1066 cycles per second, (5) a lead selenide detector and a cooling cryostat for maintaining the detector at the temperature of liquid nitrogen, (6) a tuned amplifier with a bandpass of 320 cycles per

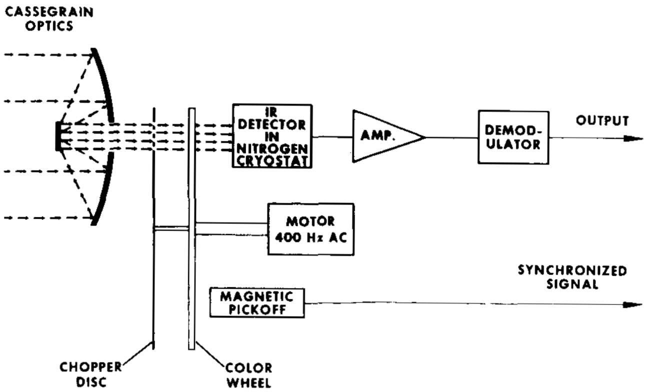

FIGURE 5. BLOCK DIAGRAM OF COLOR WHEEL RADIOMETER

second centered at 1066 cycles per second for amplifying the detector signal, (7) a half-wave rectifier and filter for converting the ac signal to dc signal, and (8) a power supply to provide both detector and amplifier bias voltages.

Figure 6 shows the spectral coverage of the filters used in the filter wheel as a function of percent transmission. These filters are mounted in the wheel and the radiometer as shown in Figure 7. The output of the radiometer for a 1000° K black body is shown in Figure 8. Figure 9 illustrates an actual output of a burning paper sheet and an infrared lamp. The instrument is calibrated with a series of black body cavities, and data reduction is accomplished by comparing the flight data with the calibration curves for each channel. The typical D* for the PbS detector is 2.5×10^{11} centimeters $\times$ (cycles per second)$^{\frac{1}{2}}$ per watt.

SCANNING GRATING SPECTROMETER

A two-channel scanning grating spectrometer was developed for MSFC and the Air Force Cambridge Research Laboratory (AFCRL) by Block Engineering Company under purchase order H-92160. The AFCRL and MSFC performed a joint measurement on the S-IB-203 vehicle to determine the signature characteristics of the S-IB engines and the spectral distribution

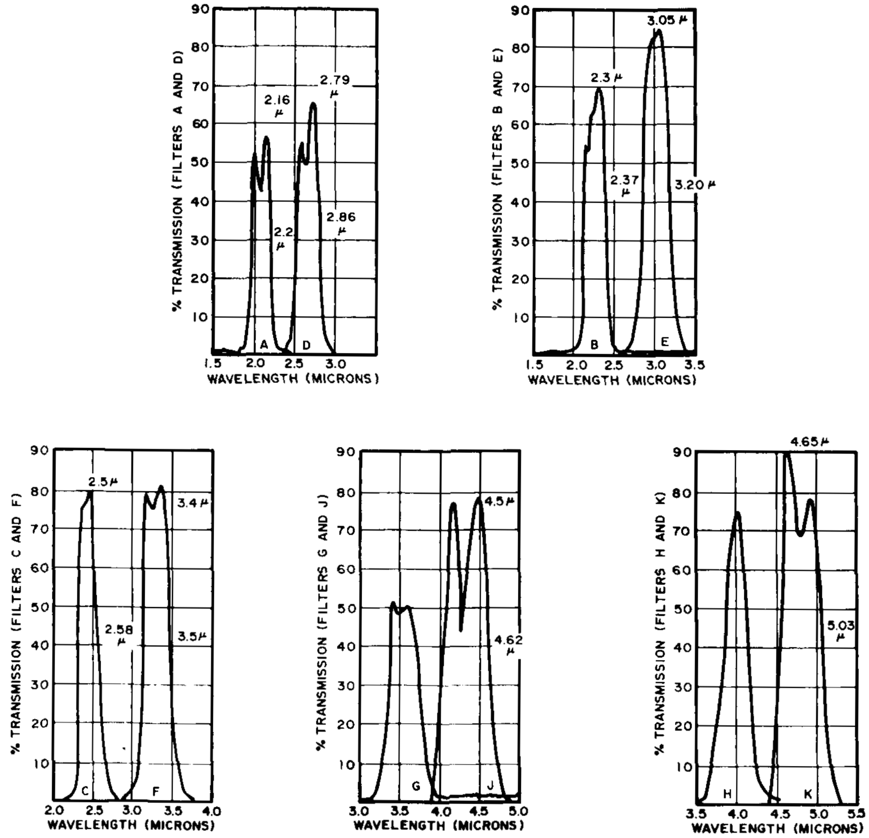

FIGURE 6. COLOR WHEEL SPECTRAL COVERAGE

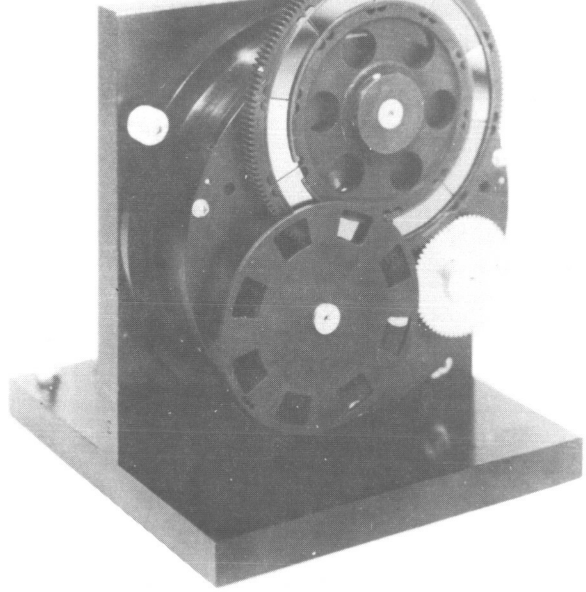

FIGURE 7. FILTER COLOR WHEEL AND RADIOMETER

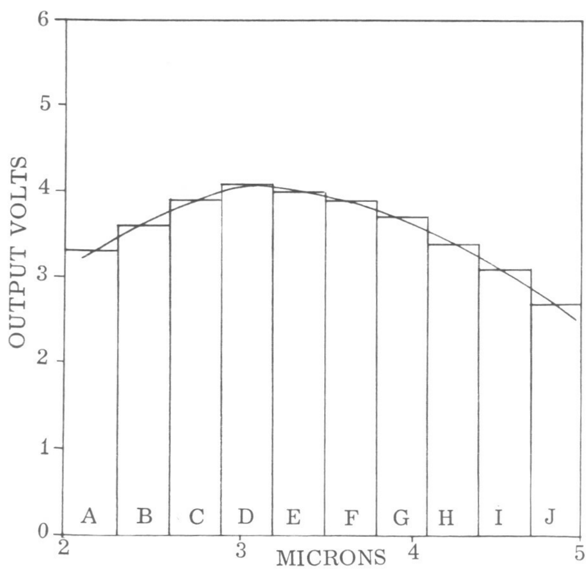

FIGURE 8. TYPICAL RADIOMETER CALIBRATION CURVE FOR 1000°K BLACK BODY

of the radiating components in the hot gases of the plume. One channel scanned the near infrared in the 1.5- to 2.3-micron spectral range. The other channel scanned the intermediate infrared in the 2.3- to 4.6-micron spectral range. The instrument was flight qualified to the Saturn IB heat shield environment.

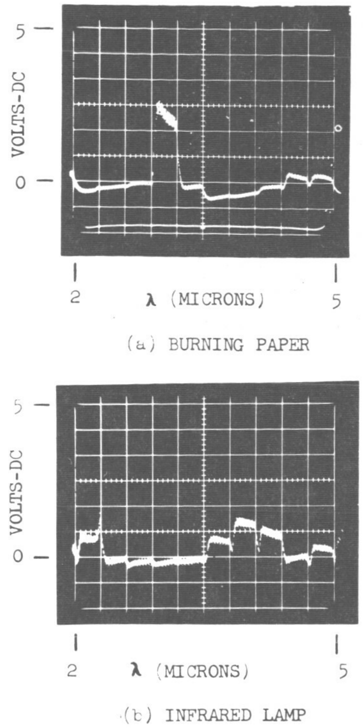

FIGURE 9. COLOR WHEEL RADIOMETER OUTPUT FOR BURNING PAPER AND INFRARED LAMP

Figure 10 is a block diagram of the spectrometer. The near infrared and intermediate infrared are functionally similar. Incident radiation entering the system is chopped and passed through a curved entrance slit to a 45 degree mirror and onto a spherical

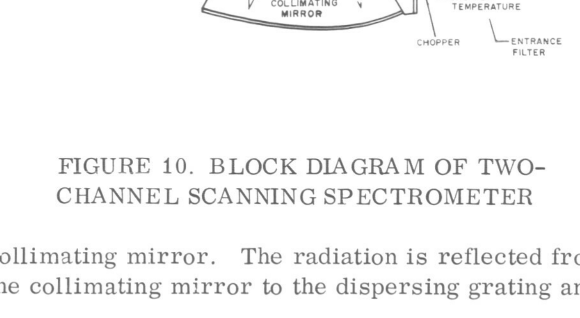

FIGURE 10. BLOCK DIAGRAM OF TWO-CHANNEL SCANNING SPECTROMETER

collimating mirror. The radiation is reflected from the collimating mirror to the dispersing grating and then back to the collimating mirror to be focused on the detector. The detector in each channel is geometrically shaped to act as an exit slit. The near IR channel uses a PbS detector and the intermediate IR channel uses a PbSe detector.

The output from each detector is preamplified and sent to a logarithmic amplifier designed to permit acceptance of inputs with a dynamic range of 5000:1. The summing circuits in the logarithmic amplifier are synchronized with the chopper by a reference light received by a solar cell through the chopper blades. Calibration lights for each channel are provided for continuous inflight reference. A typical output wave train for the system is shown in Figure 11.

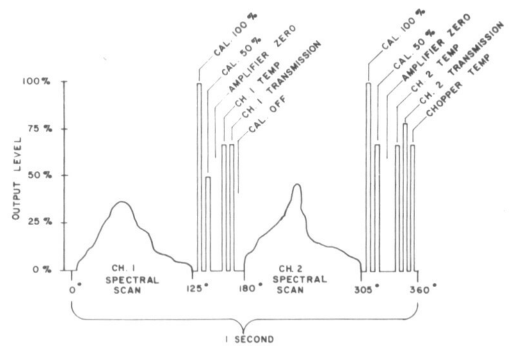

FIGURE 11. OUTPUT WAVE TRAIN FOR TWO-CHANNEL SCANNING GRATING SPECTROMETER

A summary of the system requirements is shown in Table I. The system is to scan in three angular positions of 5 degrees, 0 degrees, and -5 degrees around a reference center line. This is accomplished by mechanically stepping the spherical mirror. In each spatial position, the scanning grating is rocked through the angles necessary to scan the required 1.15- to 2.3, and 2.3- to 4.6-micron spectral ranges. The scanning rate can be adjusted, but is nominally set for one second per scan. The spectral range is scanned by the grating design and the rocking angle.

The intended application of this instrument does not require the detectors to be cooled. A nitrogen purge is provided to prevent contamination of the optical system. Figure 12 shows the instrument installed on the flight heat shield.

TABLE I. SYSTEM REQUIREMENTS FOR SCANNING GRATING SPECTROMETER

Spatial Scan	3 positions of 15 degrees (+5 degrees, 0 degrees, and -5 degrees)
Field of View	-2 degrees by 2 degrees
Spatial Scan Rate	One per second
Spectral Scans	1.1 to 2.2 microns and 2.3 to 4.6 microns
Resolution	0.1 micron
Wavelength Repeatability	+ 0.02 micron
Wavelength Accuracy	+ 0.04 micron
Dynamic Range	10^3 log
Spectral Scan Rate	Each wavelength once per second
Signal Output	0 to 5 Vdc with output impedance less than 5000 ohms
Nitrogen Purge	.0037 m/s (8 SCFM) STP, 5.2×10^6 N/m^2 (750 psi) required
Power	2 amperes ± 20% @ 28 ± 3 Vdc
Outline Dimensions	16.5 cm × 19.5 cm × 24.9 cm
Mass	11.4 kg maximum
D* PbS	1.47×10^{10} cm Hz$^{\frac{1}{2}}$/W
D* PbSe	1.8×10^7 cm Hz$^{\frac{1}{2}}$/W

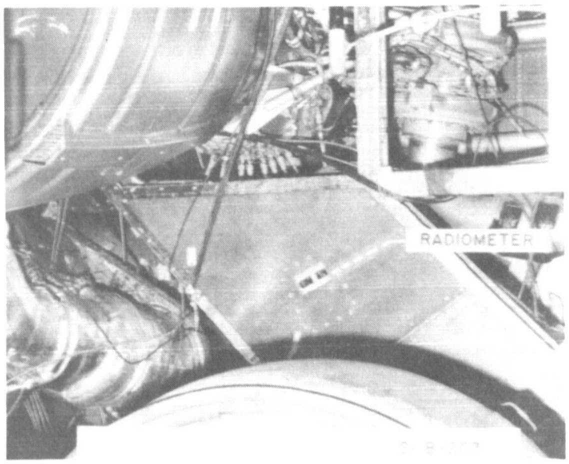

FIGURE 12. SCANNING GRATING SPECTROMETER INSTALLATION

SPECIAL SYSTEMS

A number of systems have been designed for functions that are based upon the spectral distribution of emitting sources. Marshall Space Flight Center and Rocketdyne, under NAS8-11656, have conducted a study to obtain data on the radiative characteristics of hydrogen fires and to apply these data to the design and development of a fire detection system for the upper stages of the Saturn vehicle. The system requirements were that it must discriminate against false signals from sunlight and from the rocket engine exhaust plume radiation, while subjected to the physical environments of a Saturn V vehicle.

This effort not only studied the spectral characteristics of the J-2 rocket engine exhaust radiation, but also included the following experimental investigations: (1) the effect of ambient pressure and oxygen enrichment on the likelihood of hydrogen fires and explosions, (2) possible ignition sources in the Saturn vehicle and evaluation of the hydrogen air flammability limits using such sources, (3) spectra of hydrogen air diffusion flames containing samples of materials found in Saturn vehicle compartments, (4) transmission of ultraviolet radiation through fog, smoke, and contaminants over distances typical of Saturn vehicle compartments, and (5) flicker frequency measurements of J-2 rocket engine exhaust radiation.

The hydrogen fire detection system in Figure 13 will respond only to time-varying radiation of appropriate wavelengths and of sufficient intensity to exceed threshold detectivity. The system will discriminate between hydrogen air fires and time-varying or steady-state sunlight.

The detection system consists of (1) the radiometer, in which time-varying ultraviolet and visible radiation is photoelectrically detected, and (2) the control unit in which the produced electronic signals are processed.

A proportional, time-varying electrical signal is generated by the radiometer when it views a source of radiation whose intensity changes with time and the emitted radiation is in the selected spectral region. A two-lens optical system, with an 8.5-degree field of view, directs radiation onto an ultraviolet-sensitive photodiode detector. Two optical filters are used to limit the detector's response to the 2600 to 3200 angstrom region characteristic of the OH molecule emission. The first filter is nickel sulfate hexahydrate and is positioned in front of the

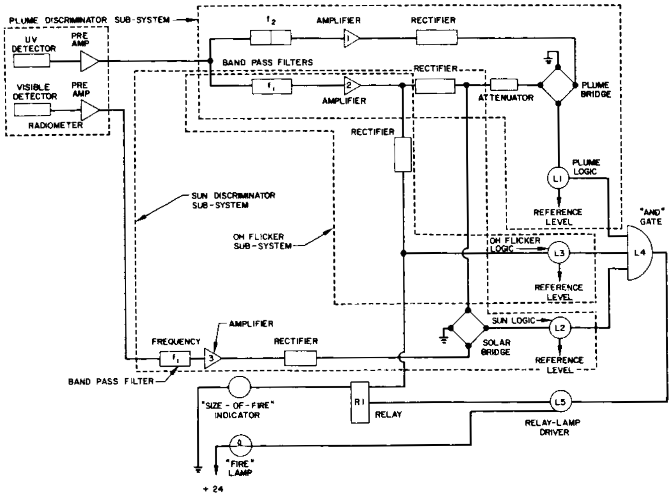

FIGURE 13. BLOCK DIAGRAM OF HYDROGEN FIRE DETECTION SYSTEM

ultraviolet detector. The second filter is made of Corning glass, Type 7-54, and is positioned between the lenses. This second filter is also a partially reflecting mirror to reflect light onto a visible photodiode detector. Electrical signals from the detectors are amplified by preamplifiers contained in the radiometer. A cross-sectional drawing of the radiometer is shown in Figure 14.

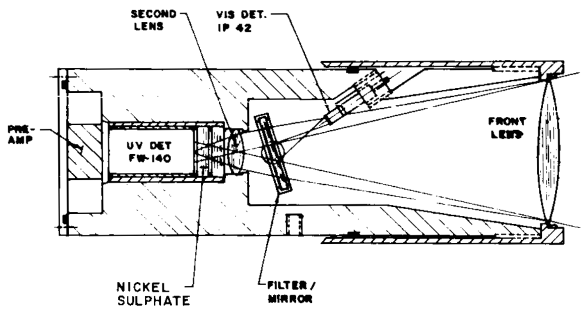

FIGURE 14. FIRE DETECTION RADIOMETER

The control unit processes the electrical signals from the radiometer. The signal processing system is composed of the sun discriminator, plume discriminator, and OH flicker.

Since the system responds only to time-varying radiation, the sun is a possible false signal source only when the sunlight is modulated by a vibrating vehicle member or by the atmosphere. Sunlight discrimination is accomplished by the two-color method which is basically the detection of the amplitude versus wavelength envelope by a two point wavelength approximation. The amplified signals from the visible detector and the ultraviolet detector are applied to separate legs of a bridge network. The other two legs of the bridge are resistances whose ratio is equal to the ratio of extraterrestrial solar radiation in the spectral bandpasses of the radiometer filters. The operation of the bridge is such that a false signal indication will be sent to the logic system for as long as the bridge sees the ratio of ultraviolet to visible radiation as that in sunlight at sea level or space vacuum. If the ultraviolet to visible radiation ratio is different, as when a hydrogen fire is observed, the output of the bridge to the logic system is a positive signal indication.

The electrical output of the two filters in the ultraviolet detector signal system are compared in a null bridge network similar to the solar bridge. When the signal source is the rocket exhaust plume, the output to the logic system indicates a false signal. If the radiation is other than the plume, the indication is positive.

In the OH flicker system, a positive indication is applied to the logic system when the time-varying ultraviolet radiation detected is of sufficient intensity. When the signal applied to the logic module is less than this value, the signal to the logic system indicates a false signal.

The hydrogen fire detection provides an indication only if the signals from the solar discriminator, plume discriminator, and OH flicker are positive. Figure 15 shows the first breadboard system. The output indication of a fire in this unit is only a meter and light, but capability exists for providing additional logic circuits for emergency detection systems.

CONCLUSION

The systems discussed have been typical of the instruments flown so far on Saturn vehicles. Proposed inflight MSFC experiments and future Apollo scientific payloads will require even more complex radiation detection and analyzing systems. Special applications of these techniques will include systems such as those required in the lunar and terrestrial mapping and surveying programs, guidance systems, horizon seekers, weather mapping, tracking of targets, surface absorptivity, emittance analysis, and surface reflectance measurements.

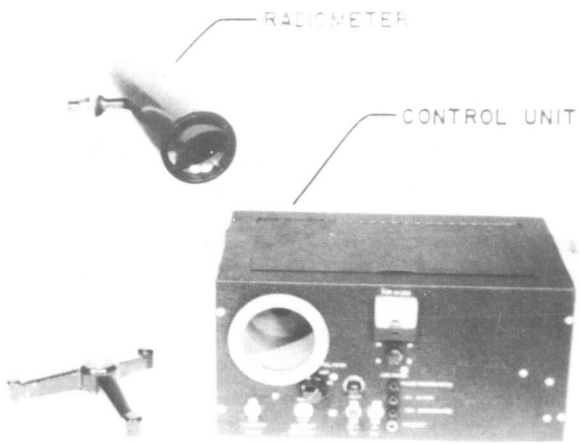

FIGURE 15. BREADBOARD HYDROGEN FIRE DETECTION SYSTEM

APPROVAL

RESEARCH ACHIEVEMENTS REVIEW
VOLUME II REPORT NO. 2

A Review of Thermophysics Research at Marshall Space Flight Center

By Gerhard B. Heller, Billy P. Jones, Edgar Miller, Gary Arnett, William C. Snoddy, and Harold Burke

The information in these reports has been reviewed for security classification. Review of any information concerning Department of Defense or Atomic Energy Commission programs has been made by the MSFC Security Classification Officer. These reports, in their entirety, have been determined to be unclassified.

These reports have also been reviewed and approved for technical accuracy.

for Gerhard B. Heller

ERNST STUHLINGER
Director, Research Projects Laboratory

UNITS OF MEASURE

In a prepared statement presented on August 5, 1965, to the U. S. House of Representatives Science and Astronautics Committee (chaired by George P. Miller of California), the position of the National Aeronautics and Space Administration on Units of Measure was stated by Dr. Alfred J. Eggers, Deputy Associate Administrator, Office of Advanced Research and Technology:

"In January of this year NASA directed that the international system of units should be considered the preferred system of units, and should be employed by the research centers as the primary system in all reports and publications of a technical nature, except where such use would reduce the usefulness of the report to the primary recipients. During the conversion period the use of customary units in parentheses following the SI units is permissible, but the parenthetical usage of conventional units will be discontinued as soon as it is judged that the normal users of the reports would not be particularly inconvenienced by the exclusive use of SI units."

The International System of Units (SI Units) has been adopted by the U. S. National Bureau of Standards (see NBS Technical News Bulletin, Vol. 48, No. 4, April 1964).

The International System of Units is defined in NASA SP-7012, "The International System of Units, Physical Constants, and Conversion Factors," which is available from the U. S. Government Printing Office, Washington, D. C. 20402.

SI Units are used preferentially in this series of research reports in accordance with NASA policy and following the practice of the National Bureau of Standards.

CALENDAR OF REVIEWS

FIRST SERIES (VOLUME I)

REVIEW	DATE	RESEARCH AREA	REVIEW	DATE	RESEARCH AREA
1	2/25/65	RADIATION PHYSICS	12	9/16/65	AERODYNAMICS
2	2/25/65	THERMOPHYSICS	13	9/30/65	INSTRUMENTATION
3	3/25/65	CRYOGENIC TECHNOLOGY	14	9/30/65	POWER SYSTEMS
*4	3/25/65	CHEMICAL PROPULSION	15	10/28/65	GUIDANCE CONCEPTS
5	4/29/65	ELECTRONICS	16	10/28/65	ASTRODYNAMICS
6	4/29/65	CONTROL SYSTEMS	17	1/27/66	ADVANCED TRACKING SYSTEMS
7	5/27/65	MATERIALS	18	1/27/66	COMMUNICATIONS SYSTEMS
8	5/27/65	MANUFACTURING	19	1/6/66	STRUCTURES
9	6/24/65	GROUND TESTING	20	1/6/66	MATHEMATICS AND COMPUTATION
10	6/24/65	QUALITY ASSURANCE AND CHECKOUT	21	2/24/66	ADVANCED PROPULSION
11	9/16/65	TERRESTRIAL & SPACE ENVIRONMENT	22	2/24/66	LUNAR AND METEOROID PHYSICS

* Classified. Proceedings not published.

SECOND SERIES (VOLUME II)

REVIEW	DATE	RESEARCH AREA	REVIEW	DATE	RESEARCH AREA
1	3/31/66	RADIATION PHYSICS	5	9/29/66	QUALITY AND RELIABILITY ASSURANCE
2	3/31/66	THERMOPHYSICS	6	1/26/67	CHEMICAL PROPULSION
3	5/26/66	ELECTRONICS	7	3/30/67	CRYOGENIC TECHNOLOGY
4	7/28/66	MATERIALS			

Correspondence concerning the Research Achievements Review Series should be addressed to: Chief, Research Program Office, R-EO-R, Marshall Space Flight Center, Huntsville, Alabama 35812.